JGR Oceans

RESEARCH ARTICLE

10.1029/2023JC020324

Drivers of Marine Heatwaves in the Arctic Ocean

Benjamin Richaud[1], Xianmin Hu[1], Sofia Darmaraki[2], Katja Fennel[1], Youyu Lu[3], and Eric C. J. Oliver[1]

[1]Department of Oceanography, Dalhousie University, Halifax, NS, Canada, [2]Coastal Marine Research Laboratory, Institute of Applied and Computational Mathematics, FORTH, Heraklion, Greece, [3]Department of Fisheries and Oceans, Bedford Institute of Oceanography, Dartmouth, NS, Canada

Key Points:

- A heat budget analysis is applied to a regional ice-ocean model to determine the dominating drivers of marine heatwaves in the Arctic
- Marine heatwaves in the Arctic provide a pathway for heat from the atmosphere to the subsurface ocean
- Sea ice melt shoals the surface mixed layer, and this prolongs and intensifies marine heatwaves

Supporting Information:

Supporting Information may be found in the online version of this article.

Correspondence to:

B. Richaud and E. C. J. Oliver,
benjamin.richaud@dal.ca;
eric.oliver@dal.ca

Citation:

Richaud, B., Hu, X., Darmaraki, S., Fennel, K., Lu, Y., & Oliver, E. C. J. (2024). Drivers of marine heatwaves in the Arctic Ocean. *Journal of Geophysical Research: Oceans*, *129*, e2023JC020324. https://doi.org/10.1029/2023JC020324

Received 1 AUG 2023
Accepted 2 FEB 2024

Author Contributions:

Conceptualization: Benjamin Richaud, Katja Fennel, Eric C. J. Oliver
Formal analysis: Benjamin Richaud, Eric C. J. Oliver
Methodology: Benjamin Richaud, Xianmin Hu, Sofia Darmaraki, Youyu Lu, Eric C. J. Oliver
Supervision: Katja Fennel, Eric C. J. Oliver
Writing – original draft: Benjamin Richaud, Eric C. J. Oliver
Writing – review & editing: Benjamin Richaud, Xianmin Hu, Sofia Darmaraki, Katja Fennel, Youyu Lu, Eric C. J. Oliver

Abstract Among the documented consequences of anthropogenic global warming are the increased frequency and duration of marine heatwaves in the global ocean. The literature dedicated to Arctic marine heatwaves corroborates those results, but fails to identify the heat sources and sinks. Because of the numerous feedbacks impacting polar regions, understanding the processes triggering and dissipating those extreme events is particularly important to predict their occurrence in a fast changing ocean. A three-dimensional regional ice-ocean numerical model is used to calculate a surface mixed layer heat budget and to investigate mechanisms generating and dissipating marine heatwaves. The majority of the marine heatwaves are onset by surface heat fluxes and decayed by bottom and surface heat fluxes. The dominant processes are spatially and seasonally heterogeneous: lateral heat flux can become the primary process when advecting heat anomalies at the main Arctic gateways or by triggering temperature extremes in winter. Using a Reynolds decomposition, it can be determined that the shoaling of the surface mixed layer induced by ice melt can significantly lengthen and intensify Arctic marine heatwaves. In winter, the analysis of marine heatwaves poses unique challenges, with the long term freshening of the Arctic inducing a positive trend of 0.1°C per decade for the freezing point. Arctic marine heatwaves are expected to keep increasing in duration and intensity due to the increased trend of the primary process, the surface heat flux, and their dissipation by bottom heat flux provides a pathway for heat from the atmosphere to the Arctic subsurface water masses.

Plain Language Summary Extreme warm temperature anomalies in the ocean, called marine heatwaves are becoming more frequent, longer and more intense around the globe. In the Arctic Ocean, the complex links between sea ice, the atmosphere and the ocean could both amplify or hinder the impact of those events. Yet, understanding where the heat comes from and where it goes is critical to anticipate further changes in an already fast-changing environment. To this aim, we calculate the sources and sinks of heat in a numerical model simulating the ocean and sea ice. Most marine heatwaves in the Arctic are generated by taking atmospheric heat up and disappear when this heat is transferred to the deeper ocean. In doing so, marine heatwaves provide a pathway for heat from the atmosphere to the subsurface ocean. Oceanic circulation can also propagate marine heatwaves along the continental shelf and toward the marginal ice zone. When ice melts, it shoals the upper layer of the ocean, concentrating the atmospheric heat and lengthening and intensifying marine heatwaves. The excess heat stored in the subsurface can be expected to resurface later in the season and will then delay the freezing of new sea ice.

1. Introduction

The region north of the Arctic Circle is warming four times faster than the global average (Rantanen et al., 2022). This fast increase of the atmospheric temperature is called *Arctic Amplification* (Bekryaev et al., 2010; Serreze et al., 2009) and is due to the strong coupling between the atmosphere, the cryosphere and the ocean. Changes on oceanic and sea ice properties are numerous and often drastic. The most publicized one is the decline of sea ice, with a strong downward trend in September ice extent of 13% per decade over the satellite era starting in 1979 and a nearly complete disappearance of sea ice older than 4 years (Meier & Stroeve, 2022; Meredith et al., 2019). The sea ice melt reduces the albedo, leading to more solar radiation absorbed by the ocean, which in turn melts more ice, leading to the positive albedo feedback (Hall, 2004). The sea ice decline in non-summer months also leads to more cloud formation, enhancing downwelling longwave radiation, here again leading to a positive cloud-sea ice feedback (Schweiger et al., 2008). New feedbacks are regularly proposed and investigated (e.g., Ivanov et al., 2016), with positive or negative influences on the Arctic Amplification (Goosse et al., 2018). In parallel, heat inflow through the Arctic gateways has increased (Docquier & Koenigk, 2021), either due to increases in

volume transport of Pacific waters (Woodgate, 2018) or in heat content of the Atlantic waters (Beszczynska-Möller et al., 2012). As a consequence, conditions in the Eastern Arctic are resembling Atlantic conditions more and more, a phenomenon called the *Atlantification* or *Borealization* of the Arctic (Muilwijk et al., 2023; Timmermans & Marshall, 2020), with consequences for the water column stratification and stability (Carmack, 2007) as well as for nutrient availability and ecosystems (Polyakov, Alkire, et al., 2020). The changes in stratification, particularly on the northward migration of the transition between the α-stratified (i.e., temperature-driven) and β-stratified (i.e., salinity-driven) ocean and on the weakening of the halocline, could have tremendous consequences. These include a potential shift from winter ice formation to deep convection if surface waters become denser than underlying waters before reaching the freezing point (Carmack, 2007; Lique et al., 2018). In addition, the increased heat inflow has led to a positive temperature trend of subsurface waters of Pacific and Atlantic origins, driving a stronger upward heat flux (HF) (Polyakov et al., 2017; Polyakov, Rippeth, et al., 2020; Timmermans et al., 2018). Associated with that is a suspected shift in the main source of ice melt, changing from atmospheric, surface melt to oceanic, basal melt (Carmack et al., 2015). Heat fluxes in the Arctic Ocean are changing, with consequences on its heat budget and on the characteristics of extreme events in the region, such as marine heatwaves (MHWs).

MHWs are anomalously warm events, with a variety of lasting ecosystem and socio-economic consequences, and have therefore recently been under the scientific and public spotlights. Hobday et al. (2016) propose a framework to define and detect MHWs as "a discrete prolonged anomalously warm water event in a particular location," during which water temperature exceeds a percentile threshold (often the 90th percentile calculated over a climatological period), for at least five consecutive days. An assessment of the evolution of MHWs in the global ocean found surface events to be more frequent, more intense and longer over the last century (Frölicher et al., 2018; Oliver et al., 2018), with strong links to anthropogenic climate change (Oliver et al., 2021). This observed, historical trend is expected to accelerate further in the next century under global warming (Fox-Kemper et al., 2021; Frölicher et al., 2018; Oliver et al., 2019). The development and dissipation of MHWs can be mechanistically driven by a wide range of physical processes linked to heat sources and sinks. Surface heat exchanges with the atmosphere (e.g., K. Chen et al., 2015; Olita et al., 2007) or potentially the sea ice, lateral heat fluxes through advection or mixing (e.g., Oliver et al., 2017) and to a lesser extent vertical heat fluxes through entrainment or mixing have been documented to drive MHWs (e.g., Holbrook et al., 2019; Oliver et al., 2021; Schlegel et al., 2021). A small number of studies have recently focused on MHWs in the Arctic Ocean (Hu et al., 2020; Huang, Wang, et al., 2021) or in adjacent seas (Carvalho et al., 2021; Golubeva et al., 2021; Mohamed et al., 2022). Those studies rely mostly on the OISSTv2.1 observational data set (Huang, Liu, et al., 2021; Reynolds et al., 2002). The long period of satellite coverage allows for a robust climatological assessment of MHW characteristics in seasonally ice-free areas. All studies document an increase in duration, frequency and intensity, and link those changes to increased atmospheric temperature and decreased sea ice coverage. A caveat of the newest version of the OISST product is the change in the calculation of sea surface temperature (SST) in partially ice-covered areas after the first of January 2016. The ice-SST regression applied in OISSTv2.0 is replaced by a freezing-point calculation in OISSTv2.1, which induces a significant offset on the shelves (Huang, Liu, et al., 2021, their Section 4c). Therefore, MHW statistics after 2016 derived from a baseline encompassing years before 2016 might be biased in partially ice-covered regions. Another limitation of surface temperature satellite observations lies in their inability to properly identify and quantify the role of individual MHW drivers (e.g., Golubeva et al., 2021; Hu et al., 2020). The description of those drivers is critical to properly understand the nature of the MHWs in the complex coupled ice-ocean environment. In particular, while sea ice is known to be an important factor in the heat budget of surface polar oceans, notably through the albedo feedback, the quantification of this importance and its role during extreme events is limited.

Given that sea ice and ocean systems are linked through numerous feedback loops (Goosse et al., 2018), identifying the influence of sea ice on the mechanisms creating and dissipating MHWs is critical. For example, Hu et al. (2020) suggest that ice melt could shoal the halocline and lead to a concentration of atmospheric HF in the mixed layer, possibly enhancing ice melt and therefore inducing a plausible but not yet validated positive feedback. Similarly, advection of warm Pacific waters through the Bering strait have triggered the onset of albedo feedback events (Timmermans et al., 2018; Woodgate et al., 2010). The strong coupling between the different climate components of the Arctic renders the disentangling of causes and consequences non-trivial, yet important to anticipate, mitigate and adapt to the impacts of anthropogenic climate change. More broadly, a proper understanding of the physical processes driving MHWs in the Arctic Ocean will help anticipate their evolution in the

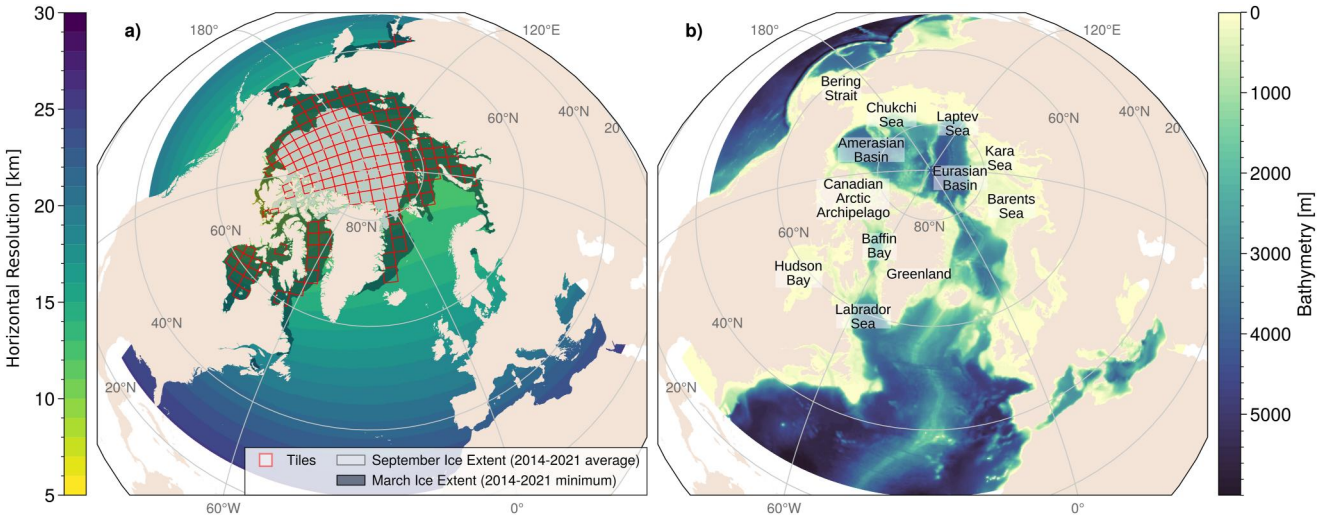

Figure 1. Maps of the region of interest. (a) Model domain and horizontal resolution (background color), model-simulated ice extent, defined as ice concentration above 15%, in March (dark gray) and September (light gray), averaged over 2014–2021, and the 160 tiles of 20 × 20 grid cells used for the analysis (red grid). (b) Model bathymetry and locations of interest; a curious reader can explore Rudels (2015) for a more in-depth and exhaustive description of the different Arctic seas, basins and ridges.

diverging scenarios for the rest of the 21st century and beyond (Fox-Kemper et al., 2021; IPCC, 2021). The future of the Arctic will have key social, cultural and economical repercussions, for example, for indigenous communities relying on Arctic ecosystems or for navigation routes.

This study aims to fill some of those gaps by using a three-dimensional ice-ocean numerical model covering the Arctic Ocean and adjacent seas from 2014 to 2021. A surface mixed layer heat budget identifies and quantifies the processes leading to the onset and decay of MHWs in the Arctic Ocean. A statistical analysis of mechanisms responsible for MHWs is provided, including the dominating role of surface HF to trigger MHWs and of bottom HF to dissipate them. The results support that MHWs provide a pathway for atmospheric heat to subsurface waters. The model, the MHW detection method and the surface mixed layer heat budget decomposition are described first (Section 2). A brief validation of the model and a description of the results are then provided (Section 3). Finally, the impacts of MHWs on the Arctic heat distribution are discussed (Section 4).

2. Methods

2.1. Model

The North Atlantic, Pacific and Arctic (NAPA) model, is a three-dimensional ocean-ice model. The ocean component is the Nucleus for European Modeling of the Ocean (NEMO, Madec et al., 2017), version 3.6. It is a finite difference, hydrostatic, primitive equation ocean general circulation model. The Louvain-la-Neuve Ice Model v3 (LIM3, Rousset et al., 2015) is a dynamic-thermodynamic ice model with one layer of snow and two layers of ice, and uses an ice thickness distribution instead of a single ice category. As its name suggests, the model covers the North Atlantic north of 26°N, the North Pacific north of 45°N and the whole Arctic, using an ORCA-like tripolar grid (Madec et al., 2017) with a nominal horizontal resolution of 1/4°, ranging from 25 km at the low latitudes to 10 km in the Canadian Arctic Archipelago (Figure 1). It is therefore eddy-permitting but not eddy-resolving. It uses z-coordinates for the vertical levels, with 75 levels in total, 9 of which are located in the first 10 m, giving the high vertical resolution necessary for simulating the shallow summer Arctic mixed layer. Outputs are written at a daily frequency. Boundary conditions are provided by GLORYS2v3 produced by Mercator Ocean (Ferry et al., 2012) and river runoff is based on monthly climatology (Dai & Trenberth, 2002). The model is forced at the surface by ERA5 (Hersbach et al., 2020) over 2014–2021 with initial conditions taken from a previous run covering 1958–2015 using the DRAKKAR Forcing Set (Dussin et al., 2016). A general validation of the model is provided in Zhang et al. (2020) and more validation specific to MHWs can be found in Section 3. We obtain daily, two-dimensional fields of ice concentration, freezing-melting flux, solar and non-solar

heat fluxes at the ocean surface, weighted according to the proportion of open and ice-covered waters, and three-dimensional fields of seawater temperature, salinity, u- and v- velocities.

2.2. Marine Heatwaves

Extreme events can be defined using a range of methods. Classic methods are often based on return periods or peaks over threshold (Coles, 2001). In the context of MHWs, a wide-spread and generally accepted definition has been provided by Hobday et al. (2016) and uses a peak-over-threshold definition without assuming an underlying probability distribution for the events. This methodology is applied here to the modeled mixed layer temperature, from 2014 to 2021. We discuss the impact of using this relatively short time series, compared to the recommended 30-year time series, in Section 4. A daily climatology of temperature is first calculated over an 11-day window then smoothed with a 31-day rolling average. A MHW is defined as an anomalously warm event persisting at least 5 days above the daily 90th percentile. Gaps between events of 2 days or less followed by a 5 days or longer event are ignored. The peak of an MHW is defined as the temperature maximum relative to the threshold, the "onset" is defined as the period between the first day of the MHW and the peak, while the period between the peak and the last day of the MHW is called the "decay." This definition has been implemented in different software packages, including Python (https://github.com/ecjoliver/marineHeatWaves). Considering the very stable conditions in the Arctic Ocean during winter, with surface water temperatures at the freezing point for several months, the 90th percentile threshold can be very close to the climatological mean and a very small departure from the freezing point (of the order of a few hundredth of a Celsius degree) can lead to the detection of an MHW. The biological and physical significance of such events are yet to be determined. While some Arctic studies add an absolute, summer-based value threshold condition to circumvent that issue (e.g., Huang, Wang, et al., 2021), we rather filter MHWs based on their intensity. More specifically, an Arctic MHW has a mean intensity relative to the climatological mean that exceeds a chosen value of 0.1°C. The number of detected MHWs is not very sensitive to the intensity threshold value, especially in summer. A lower value would include more winter, small amplitude MHWs that we aim to discard, while a higher value would eliminate some of the shoulder seasons and summer MHWs, that could be considered as relevant (Figure S1 in Supporting Information S1). The importance and processes related to the winter MHWs are discussed later (Section 4).

The MHW detection algorithm is not run on individual grid cells but rather on tiles of 20 by 20 grid cells, and tiles with less than 300 grid cells are discarded. One benefit of calculating the heat budget over tiles is to avoid the impacts of lateral eddy viscosity that may be large for individual grid cells. Another benefit is that the occurrence MHWs between individual tiles are less correlated than that between individual grids. The mixed layer temperature of a grid cell is strongly correlated with the temperature of the surrounding grid cells and this correlation was found to decrease for grid cells further than 10 grid cells away, although with strong spatial variability (not shown). Using tiles of 20 by 20 grid cells thus increases the independence between detected MHW events at adjacent tiles. The tiles are further filtered out by excluding tiles where the March ice concentration never exceeds 15% in the 2014 to 2021 period, to constrain our study on seasonally ice-impacted regions (Figure 1a, dark shade). A total of 160 tiles were found to match those criteria. For the remainder of the study, we restrain our definition of the Arctic Ocean to the area covered by those tiles.

2.3. Surface Mixed-Layer Heat Budget

In order to isolate the different drivers of each MHW, a surface mixed layer heat budget is calculated. While the NEMO model calculates mixed layer depth as an output variable, its definition is not suited to the Arctic Ocean. The model mixed layer depth is defined as the depth where there is a potential density difference of 0.01 kg m^{-3} with respect to the density at 10 m depth, meaning the mixed layer depth cannot be shallower than 10 m. Yet, because of the strong stratification due to ice melt, the summer Arctic surface mixed layer is regularly observed to be significantly thinner than 10 m (Peralta-Ferriz & Woodgate, 2015). In order to better match observational mixed layer values and modeled stratification, we redefine the surface mixed layer depth as the depth at which the potential density exceeds 0.05 kg m^{-3} with respect to the density at 5 m depth. This new definition provides a realistic simulation of the summer mixed layer with negligible differences to the original NEMO mixed layer depth in other seasons (not shown). A heat budget can then be calculated for this mixed layer.

In general, over a fixed area, the rate of change of the averaged mixed layer temperature can be written as (Moisan & Niiler, 1998; Oliver et al., 2021)

$$\frac{\partial \langle T \rangle}{\partial t} = \underbrace{-\langle \mathbf{u} \rangle \cdot \nabla \langle T \rangle + \langle \nabla \cdot (\kappa_h \nabla T) \rangle}_{\mathcal{Q}_{lat}} \underbrace{-\frac{1}{H} \kappa_z \frac{\partial T}{\partial z}\Big|_{-H} - \left(\frac{\langle T \rangle - T|_{-H}}{H} \right) \left(\frac{\partial H}{\partial t} + \mathbf{u}|_{-H} \cdot \nabla H + w|_{-H} \right)}_{\mathcal{Q}_{bot}} + \underbrace{\frac{F_{surf}}{\rho_0 c_p H}}_{\mathcal{Q}_{surf}} \tag{1}$$

with T the mixed layer temperature (here in °C), H the mixed layer depth (in m), $\frac{\partial T}{\partial t}$ the temperature tendency (here in °C s^{-1}), $\mathbf{u}$ the horizontal velocity vector and w the vertical velocity (here in m s^{-1}), ∇ the horizontal gradient operator, κ_h and κ_z the horizontal and vertical diffusivity coefficients (here in m^2 s^{-1}), ρ_0 the seawater density taken constant at 1,026 kg m^{-3}, c_p the seawater heat capacity taken constant at 3,991.9 J kg^{-1} $°C^{-1}$ (Madec et al., 2017) and F_{surf} the surface HF (in J s^{-1} m^{-2}). The bracket notation refers to vertical averaging of the quantity $\langle x \rangle = \frac{1}{-H} \int_{-H}^{0} x dz$. For a discussion on the dynamical relevance of those terms in the context of MHWs, see Oliver et al. (2021). In order to maintain a concise and simple interpretation of the evolution of the mixed layer temperature, the heat budget is simplified by grouping terms together as the lateral HF $\mathcal{Q}_{lat}$, the bottom HF $\mathcal{Q}_{bot}$ and the surface HF $\mathcal{Q}_{surf}$. The surface HF encompasses thermal (longwave) and solar (shortwave) radiations, as well as sensible and latent heat fluxes, surface weighted between air-sea (open water) and ice-sea (ice-covered ocean) areas. The calculation for the heat budget is done offline, using the daily outputs from the NAPA model. Some diagnostic variables were not written out, including those necessary to calculate the vertical mixing and the lateral eddy diffusivity and the offline calculation leads to numerical noise. In consequence, the budget cannot be perfectly closed and leads to some residuals $\mathcal{Q}_{resi}$. The mixed layer temperature equation thus becomes

$$\frac{\partial \overline{T}}{\partial t} = \mathcal{Q}_{lat} + \mathcal{Q}_{surf} + \mathcal{Q}_{bot} + \mathcal{Q}_{resi} \tag{2}$$

To circumvent the lack of vertical mixing and advection calculation due to missing model outputs, a two-layer heat budget is proposed: a first heat budget is calculated for the lower layer encompassing the water column between the mixed layer depth and the ocean floor as

$$\frac{\partial \overline{T^{low}}}{\partial t} = \mathcal{Q}_{lat}^{low} + \mathcal{Q}_{surf}^{low} \tag{3}$$

with $\overline{T^{low}}$ the vertically-averaged temperature of the lower layer and $\mathcal{Q}_{lat}^{low}$ the lateral HF for the lower layer. For the lower layer of the water column, the bottom HF is null (geothermal fluxes are neglected in the present configuration). $\mathcal{Q}_{surf}^{low}$ is the HF at the interface between the mixed layer and the lower layer of the water column and is therefore the opposite of the bottom HF of the mixed layer: $\mathcal{Q}_{surf}^{low} = -\mathcal{Q}_{bot}$. It accounts for vertical mixing, entrainment (including mixed layer tendency, lateral induction and vertical advection) and solar radiation penetrating deeper than the mixed layer and cannot be entirely calculated, as mentioned above. Yet, it can be evaluated using Equation 3 and re-injected in the mixed layer heat budget (Equation 2).

Following this tiling process, the remaining residuals are found to be small. They can nonetheless be used to constrain uncertainties on the heat budget and the relative influence of each term. To do so, the residual term is entirely attributed to the temperature tendency or heat fluxes terms, one after the other, providing upper and lower bounds for each term (see Supporting Information S1).

2.4. Reynolds Decomposition of Surface Heat Flux

In order to better analyze the relative contribution of each term to the MHWs, heat budget anomalies are calculated by decomposing each term X in a slowly varying part $\overline{X}$ (the climatology) and a perturbation X' defined such that $\overline{X'} = 0$, as in a Reynolds decomposition. Equation 2 then becomes

$$\frac{\partial\left(\overline{T}+T'\right)}{\partial t} = \frac{\overline{\partial T}}{\partial t} + \frac{\partial T'}{\partial t} = \overline{\mathcal{Q}_{\text{lat}}} + \mathcal{Q}'_{\text{lat}} + \overline{\mathcal{Q}_{\text{surf}}} + \mathcal{Q}'_{\text{surf}} + \overline{\mathcal{Q}_{\text{bot}}} + \mathcal{Q}'_{\text{bot}} + \overline{\mathcal{Q}_{\text{resi}}} + \mathcal{Q}'_{\text{resi}} \tag{4}$$

Since an MHW is an extreme deviation from the climatology, we focus on the anomalies and the equation of interest is

$$\frac{\partial T'}{\partial t} = \mathcal{Q}'_{\text{lat}} + \mathcal{Q}'_{\text{surf}} + \mathcal{Q}'_{\text{bot}} + \mathcal{Q}'_{\text{resi}} \tag{5}$$

By integrating Equation 5 separately over the onset and the decay, one can determine the heat sources and sinks that trigger or dissipate the extreme event and rank them for each MHW. The dominant process, contributing the most as a source during the onset (or as a sink during the decay), is called the primary process; the next contributing process is called secondary; we disregard the tertiary and higher processes for the remainder of this study.

When applying Equation 2 to the surface mixed layer, the surface term is proportional to the ratio between the surface HF and the mixed layer depth H:

$$\mathcal{Q}_{\text{surf}} = \frac{F_{\text{surf}}}{\rho_0 c_p H}$$

As mentioned earlier (Section 1), the shoaling of the mixed layer has been hypothesized to concentrate atmospheric HF and facilitate the emergence of an MHW. In order to investigate the relative contributions of surface HF and mixed layer change in the density of heat input in the surface mixed layer, $\mathcal{Q}'_{\text{surf}}$ can be further decomposed into contributing components. We find that

$$\mathcal{Q}'_{\text{surf}} = \frac{1}{\rho_0 c_p} F'_{\text{surf}} \overline{\frac{1}{H}} + \frac{1}{\rho_0 c_p} \overline{F_{\text{surf}}} \left(\frac{1}{H}\right)' + \frac{1}{\rho_0 c_p} \left(F'_{\text{surf}} \left(\frac{1}{H}\right)'\right)' \tag{6}$$

For details, see Appendix A.

A hypothetical temperature with no shoaling T^{ns} can be evaluated by removing the contribution of shoaling from the temperature tendency:

$$\frac{\partial T^{\text{ns}}}{\partial t} = \frac{\partial T}{\partial t} - \frac{1}{\rho_0 c_p} \overline{F_{\text{surf}}} \left(\frac{1}{H}\right)' \tag{7}$$

which, when integrated from the beginning of the MHW t_0 to some day t_1 and assuming that $T^{\text{ns}}(t = t_0) = T(t = t_0)$, leads to

$$T^{\text{ns}}(t = t_1) = T(t = t_0) + \int_{t_0}^{t_1} \left(\frac{\partial T}{\partial t} - \frac{1}{\rho_0 c_p} \overline{F_{\text{surf}}} \left(\frac{1}{H}\right)'\right) \mathrm{d}t \tag{8}$$

Similar calculation can be conducted by including the last term of Equation 6 to obtain another estimate of the temperature with no shoaling influence, $T^{\text{ns}}*$:

$$\frac{\partial T^{\text{ns}*}}{\partial t} = \frac{\partial T}{\partial t} - \frac{1}{\rho_0 c_p} \overline{F_{\text{surf}}} \left(\frac{1}{H}\right)' - \frac{1}{\rho_0 c_p} \left(F'_{\text{surf}} \left(\frac{1}{H}\right)'\right)' \tag{9}$$

The MHW algorithm (see Section 2.2) can then be applied to the new time series to estimate the influence of ice-melt induced shoaling on the MHW (Section 3.4).

3. Results

3.1. Case Study: The 2020 Siberian Heatwave

In the summer of 2020 an intense atmospheric heatwave occurred over Siberia, breaking several temperature records and leading to notable forest fires (Ciavarella et al., 2021; Overland & Wang, 2021). A concurrent intense MHW can be observed from satellite data products such as OISSTv2.1 (Figure 2a, gray dashed line, and Figure S2 in Supporting Information S1) (cf. also the MHW Tracker, http://www.marineheatwaves.org/tracker.html; Schlegel, 2020). This MHW is well reproduced by the NAPA model and exhibits similar behavior, reaching a first peak early June, a second peak in the first half of July, a third peak early August and a fourth peak end of August (Figure 2a). While the satellite-derived OISSTv2.1 product provides SST (Figure 2a, gray dashed line), our study examines the MHW over the mixed layer (Figure 2a, black line), leading to a difference in the intensity simulated by the model. This, associated with a difference of the baseline used to calculate the threshold, leads to the detection of 4 MHWs in our analysis, while Huang, Wang, et al. (2021) only detect one, long MHW (see their Figure 1). The local maxima are similar between both products, though the first peak from our model does not exceed the threshold for the OISSTv2.1 product and is therefore not included in the MHW detected by the satellite-derived product.

The spatial evolution of the MHW in the NAPA model (Figures 2e–2i) is also consistent with the observed spatial extent provided by OISSTv2.1 (Figure S2 in Supporting Information S1). A strong positive temperature anomaly starts on the eastern part of Kara Sea in July, then intensifies over the Laptev Sea while decreasing in the Kara Sea in August. Then the anomaly spreads over a large area encompassing Barents, Kara and Laptev Seas in September to decay in October, except in the Laptev Sea. While the temperature anomalies are quantitatively similar in both products (note the difference in colorbar), there are some discrepancies, with the MHW (area without hatches) more widespread in the NAPA model than in the OISSTv2.1 product. This could be related to a lower threshold for the mixed layer temperature, compared to the SST (we use the same baseline period for both products here). There is also a significant difference in the ice extent, with ice melting faster in the NAPA model than in the OISSTv2.1. The reanalysis product ERA5, used to force the model, is known to have a warm bias in the Arctic that could lead to excessive ice melt (Batrak & Müller, 2019). It should also be noted that OISSTv2.1 does not observe ice concentration directly but rather uses a set of merged products, potentially leading to biases (Reynolds et al., 2007).

According to the model, all four onsets are primarily due to the strong atmospheric HF into the ocean (Figures 2b and 2c) in consistency with the existence of the atmospheric heatwave at this time. The decays of each MHW are led by different processes, with the first and third MHWs fading mostly due to bottom flux, the second one being mainly cooled down by surface flux despite a strong source of heat from the bottom and the fourth MHW is dissipated by lateral advection with some heat lost to the subsurface (Figures 2b and 2d). The decay of the second MHW is co-occurring with a decrease of the air temperature to 4.5°C on the 13 July 2020 and less incoming solar radiation according to the ERA5 reanalysis product (not shown), explaining the anomalous atmospheric sink of heat. The heat budget analysis provides a detailed description the mechanisms behind this specific event but can also be used to obtain a general overview of the main processes for all MHWs in the Arctic Ocean.

3.2. Detected Arctic Marine Heatwaves and Dominant Processes

We then apply our method to the entire Arctic domain. We detect a total of 923 MHWs in all seasons between 2014 and 2021, the majority of them occurring in summer. The characteristics of those MHWs are spatially variable, with the maximum mean intensity occurring at lower latitudes and on the shelves (Figure 3c). The Hudson Bay and Kara Sea in particular see mean intensities exceeding 2.5°C (see Figure 1b for the location of the most regularly mentioned places in this study). The longest MHWs occur on the Siberian Shelves (including Kara, Laptev and Chukchi Seas) and over the Eurasian Basin, as well as in Baffin Bay, with MHWs that last over 40 days on average (Figure 3b). This is consistent with satellite-derived MHWs (Huang, Wang, et al., 2021). The number of days per year experiencing MHW conditions differs from the mean duration, as it is higher around Svalbard, in Baffin Bay and at the Pacific gateway, in Chukchi Sea (Figure 3a). The main difference, occurring in the Eurasian Basin where the mean duration is the longest and the number of MHW days is average, is due to a

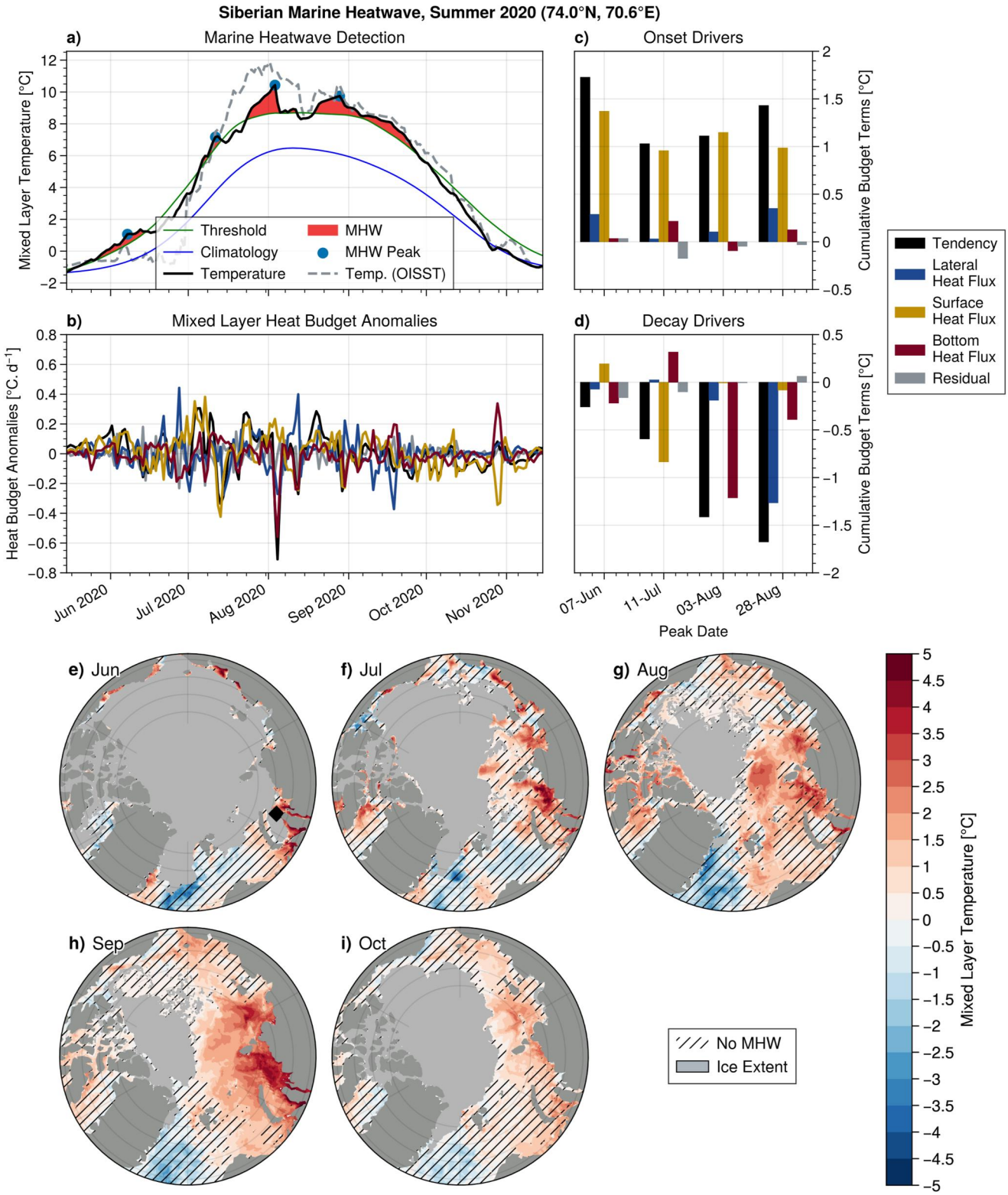

Figure 2.

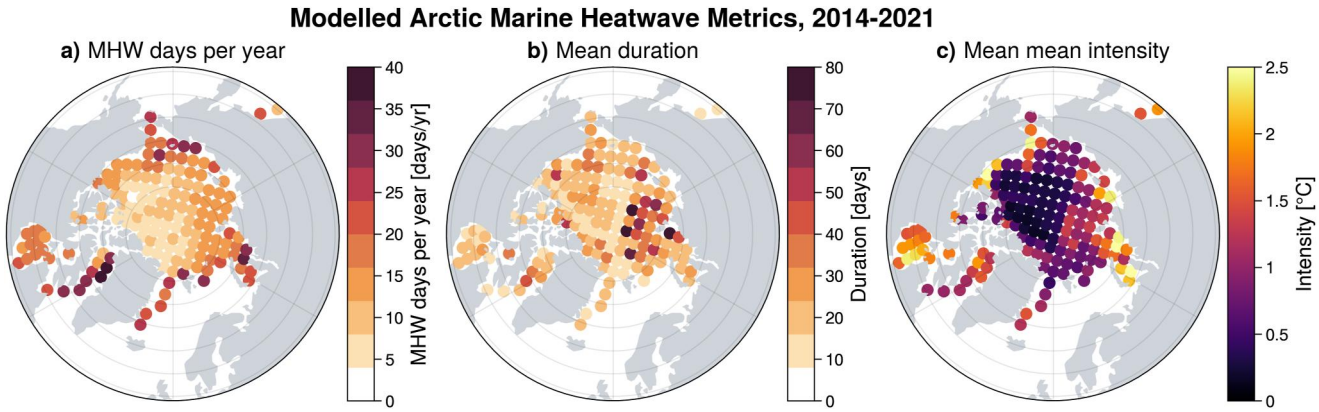

Figure 3. Commonly used marine heatwave metrics averaged over each analyzed tile (dots): average number of days per year experiencing an marine heatwave (MHW) (a), mean duration (b) and average mean intensity (c) of MHWs relative to climatology for the period extending from 2014 to 2021, for the simulated MHWs.

lower number of longer MHWs in that region. The good match with the currently published literature provides confidence that the model is simulating realistic MHWs and is therefore likely to provide a useful description of the main processes.

We apply the analysis presented for the 2020 Siberian MHW (Section 3.1) to all tiles and detected MHW events. Two thirds of the modeled MHWs (between 66% and 69%) are onset by surface HF, while the rest of the MHWs are equally triggered by lateral advection and by bottom HF (Figure 4a). Lateral advection plays an important role nonetheless, being the secondary process in 52%–56% of the MHWs (Figure 4b). The decay shows a different picture, with the highest number of MHWs being primarily dissipated by bottom HF (43%–45%), closely followed by surface HF (40%–41%) (Figure 4d). Lateral advection primarily dissipates only 15%–16% of the MHWs, but once again plays a significant secondary role for 38%–40% of them (Figure 4e). This gives an overall picture of MHWs with different sources and sinks of heat during their onset and decay. The small spread in those estimates show the small amplitude of residuals and therefore give confidence in the heat budget (Figure 4, black whiskers). This general description of MHWs in the Arctic Ocean provides an overall picture of the mechanisms at play. There remains the potential for temporal and spatial variability of the dominating processes.

3.3. Marine Heatwave Processes: Spatio-Temporal Variability

The occurrence of MHWs and their dominating processes for the onset and the decay differ strongly between seasons (Figure S3 in Supporting Information S1). The winter (January to March) MHWs are scarce, amounting to only 69 (7% of the total), but exhibit a contrast with the general overview provided earlier. Only 10% of them are driven by the surface flux, while 48% are triggered by lateral advection and 42% by bottom flux. The winter events are also mostly dissipated by surface flux (51%), in line with the expectation of cold atmospheric conditions and ice formation. The three other seasons (spring, April to June, with 107 MHWs, summer, July to September, with 591 MHWs and fall, October to December, with 156 MHWs) all show a dominance of the surface HF for triggering the extreme events, but while spring and summer match the general picture of decay being dominated by bottom flux, fall MHWs exhibit a sharp difference, with most events (70%) being dissipated by the surface HF, in line with the above-mentioned expectation of a cooling atmosphere and freezing conditions.

Figure 2. Illustration of the heat budget decomposition for the modeled Siberian Marine Heatwave of Summer 2020. This event was detected as four separate marine heatwaves. (a) Detection of the Marine Heatwaves (red) and their peaks (blue dot), when the surface mixed layer temperature (black line) exceeds the 90th percentile (green line); the climatology is also indicated (blue line), along with sea surface temperature from OISSTv2.1 product, for comparison (gray dashed line). (b) Time series of the main heat budget terms and their cumulative role for the (c) onset and the (d) decay of each of the four detected marine heatwaves (MHWs) (temperature tendency in black, lateral advection in blue, surface heat flux (HF) in yellow, bottom HF in red, residuals in gray). (e–i) Spatial evolution of the modeled MHW over the Summer 2020. Each map is a snapshot of the mixed layer temperature anomaly on the 15th of the month (background colors), superimposed by the ice extent (ice concentration higher than 15%, gray area). Areas with no detected MHW are also indicated (hatches). The model data shown here agree well with the satellite observations (Figure S2 in Supporting Information S1). The tile illustrated in panels (a–d) is shown as a black square in panel (e).

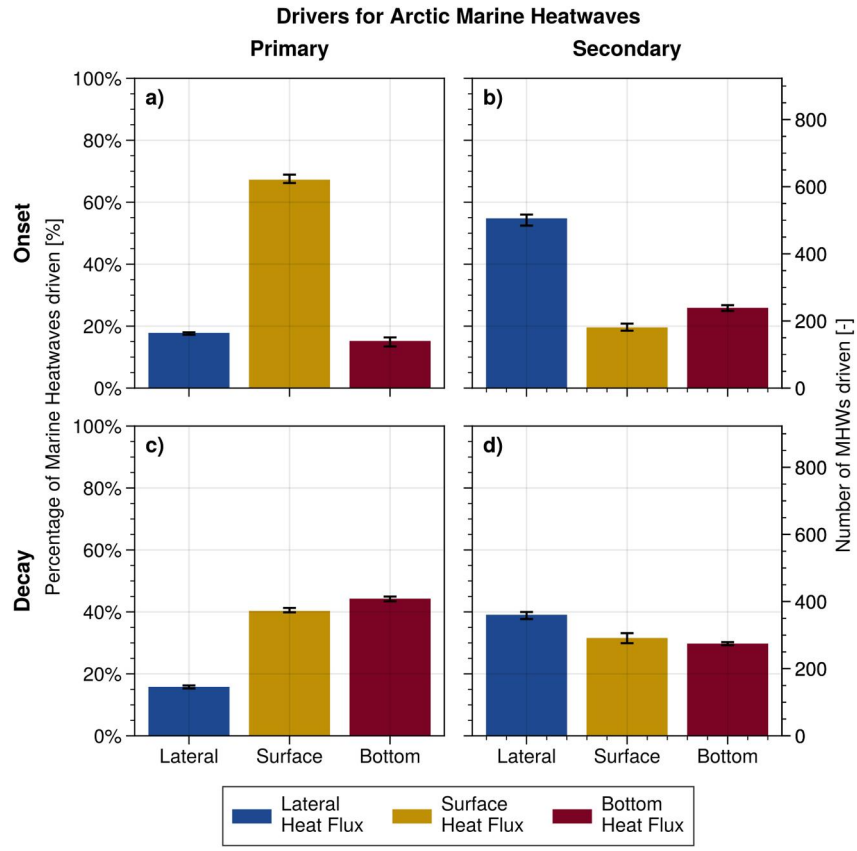

Figure 4. General overview of the primary (a, c) and secondary (b, d) processes for all detected marine heatwaves (MHWs) during the onset (a, b) and decay (c, d). Percentages are based on the total number of events detected in the numerical simulation over the Arctic Ocean between 2014 and 2021. Whiskers show the full range of the number of driven MHWs, when accounting for residuals as a measure of uncertainty.

The existence of an MHW during freezing conditions is counter-intuitive and could be deemed paradoxical. To explore the possibility for such an occurrence, a complementary view is provided by clustering the onset and decay of MHWs by ice-ocean freshwater flux (Figure S4 in Supporting Information S1). A positive flux means the ice is melting. An arbitrary threshold of 1 kg of water per squared meter is used to divide between three states: melt, freeze and no ice. Most MHWs detected in this study occur in melting conditions (61% for the onset, 53% for the decay) and a third of them occur with no ice melt nor freeze. Surprisingly, a non-negligible number (8%) of MHW onsets occur while the ice is freezing and twice more MHWs (16%) are dissipated in those ice conditions. An obvious explanation for the co-occurrence of an MHW and freezing conditions is the use of the relatively large tiles (around 200 by 200 km), which can agglomerate spatially diverse conditions. Another potential explanation is the use of the mixed layer temperature to detect MHWs: while the temperature should theoretically be homogeneous in this layer, it is not always the case in practice and in a few rare instances those MHWs are occurring at the subsurface while the ice is freezing at the top (not shown). The role of the freshening of the Arctic Ocean on the detection of MHWs is also discussed in Section 4. Overall, the dominant processes of MHWs follow the same progression as previously described, with the surface HF being dominant for the onset when the ice is melting or gone and bottom HF dominating the dissipation of MHWs. The ice condition clustering does provide complementary information about the dissipation of MHWs, with bottom flux being more strongly dominant in no-ice or melting conditions. Surface HF dissipates most MHWs when the ice is freezing, unsurprisingly. The lateral advection triggers over 60% of the MHWs when the ice is freezing, while around 30% of those are due to bottom flux, supporting the hypothesis of spatially (horizontally or vertically) heterogeneous conditions to explain the presence of MHWs during freezing conditions. The presence of sea ice is not only a seasonal pattern, but also follows a latitudinal gradient.

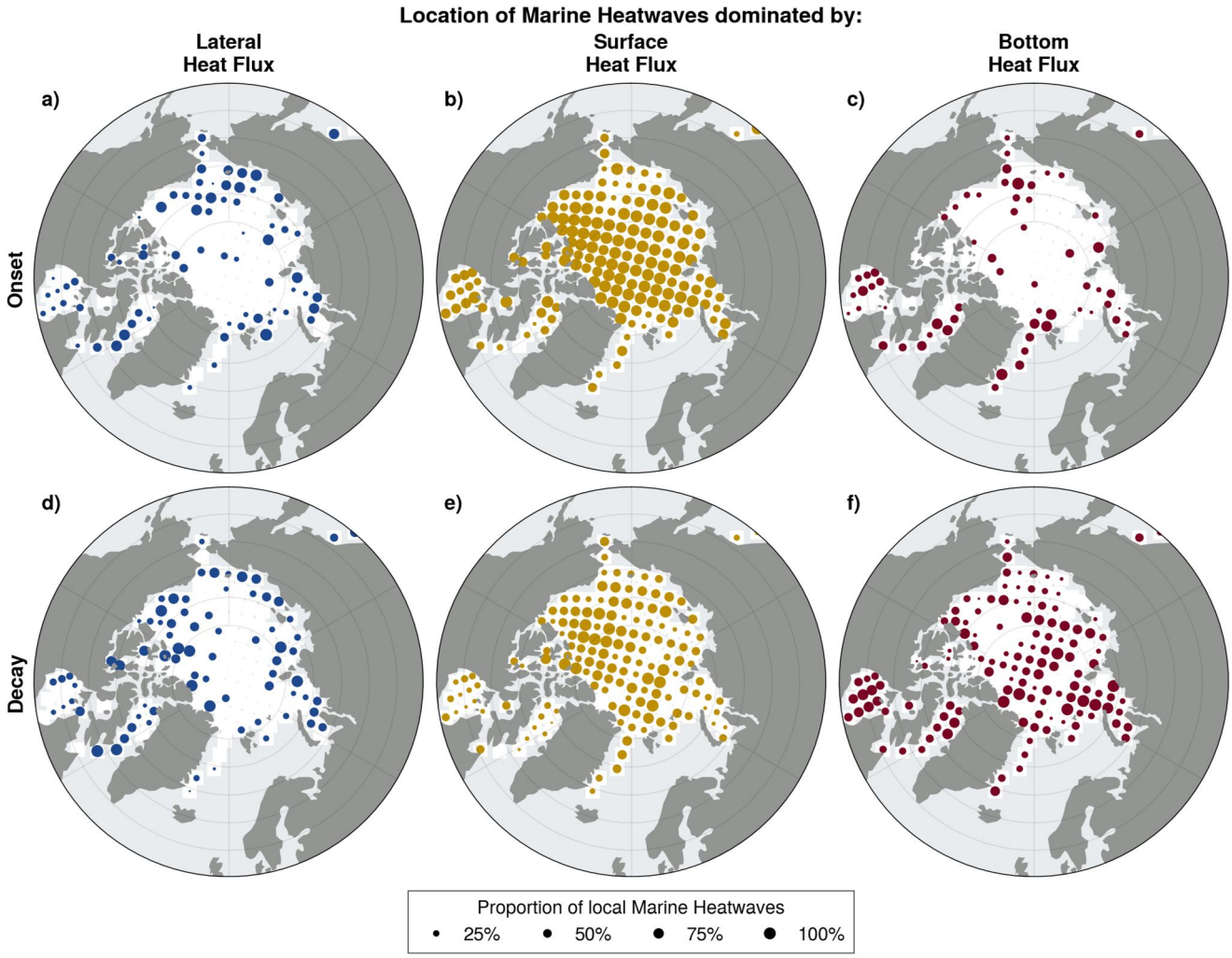

Figure 5. Geographic distribution of the marine heatwaves (MHWs) primarily driven by lateral (a, d), surface (b, e) or bottom (c, f) heat fluxes, for the onset (a–c) and the decay (d–f), according to the NAPA model. Each dot represents a tile and the size of the tile shows the proportion of the detected MHWs for that specific tile that are driven by either lateral, surface or bottom HF; a white space means none of the detected MHWs in that tile are primarily driven by the associated HF; pale gray regions indicate locations not covered by this study.

The patterns of the dominant processes of Arctic MHWs are reflected spatially as well (Figure 5). The surface HF is the dominant onset process over most of the Arctic Ocean, except north of Bering Strait, in Baffin Bay and along the eastern shore of Greenland, where it shares the role of triggering MHWs with either the bottom HF, or with the lateral advection term in Baffin Bay and north of Bering Strait. During the decay phase, the surface HF clearly plays a smaller role, though still important everywhere. The bottom HF plays a limited role during the onset, apart from the above-mentioned regions, and is a dominant process for the decay over most of the Arctic, especially in Baffin Bay, Kara Sea, the Eurasian Basin and Hudson Bay. It is worth noting the absence of bottom dissipation of MHWs in the Beaufort Gyre, further discussed in Section 4. The role of lateral advection exhibits strong spatial patterns, mostly constrained to the shelves and Baffin Bay. Regions where onset and decay are primarily driven by lateral advections are similar. Those locations are mostly consistent with known oceanographic features, such as the northward inflow of warm Pacific waters through Bering Strait, the inflow of warm Atlantic waters through the Barents Sea Opening, the recirculation of the West Greenland boundary current in Baffin Bay and north of the Labrador Sea, or the anticyclonic Beaufort Gyre in the Central Arctic Ocean, which would bring cold waters southward from the North Pole along the Canadian Arctic Archipelago to the Beaufort Sea. This explains the importance of the advective term in this area during the decay, while being limited during the onset.

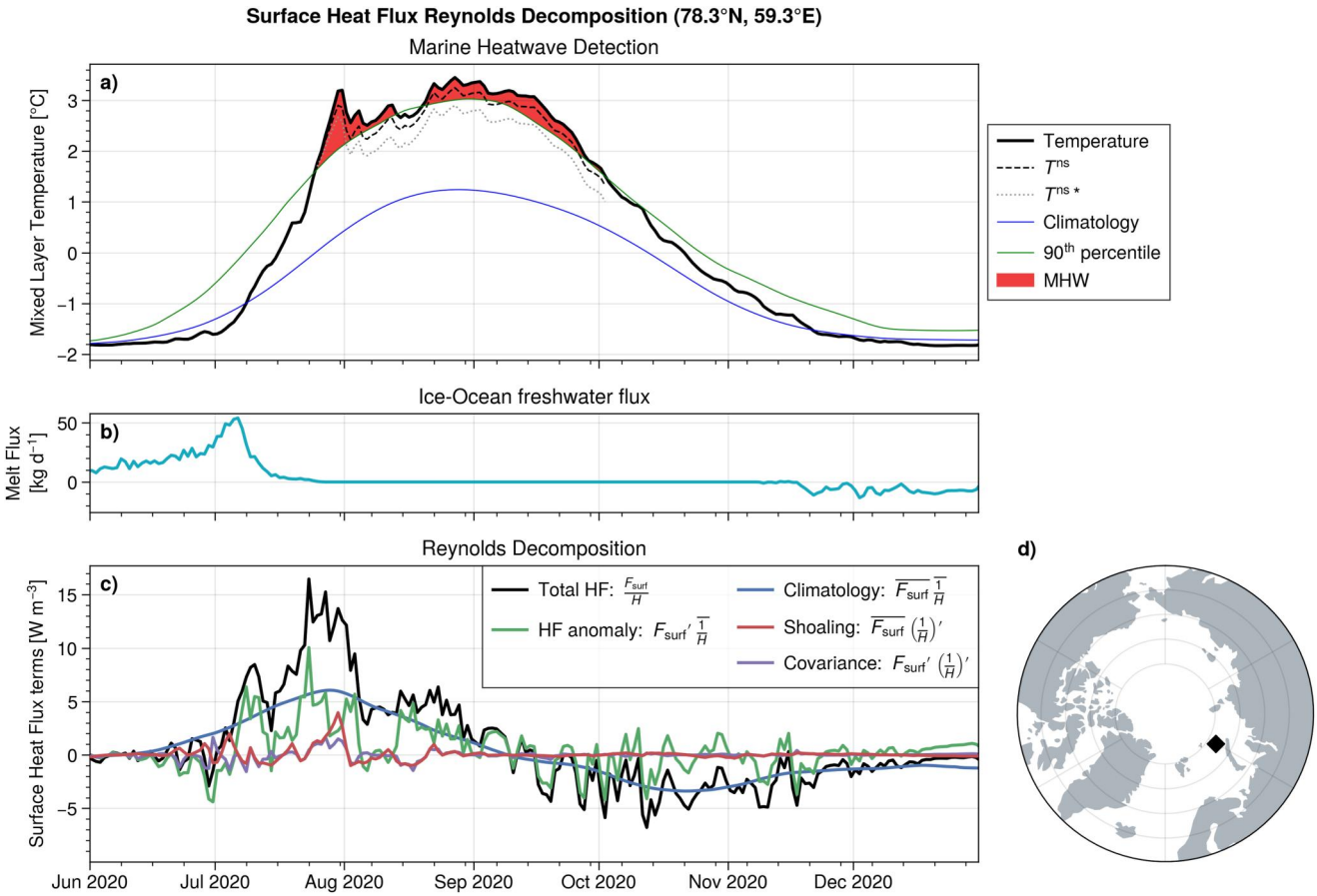

Figure 6. Illustration of the Reynolds decomposition of the surface heat flux (HF) during the summer 2020 Siberian Heatwave. (a) Detection of the marine heatwave (MHW) (red) when the modeled mixed layer temperature (black line) exceeds the 90th percentile (green) and impact of the mixed layer shoaling on the MHW when the shoaling term $\overline{F_{surf}}\left(\frac{1}{H}\right)'$ is excluded (T^{ns}, black dashes; see Equation 7) and when both shoaling and covariance $\overline{F_{surf}}\left(\frac{1}{H}\right)' + \left(F_{surf}'\left(\frac{1}{H}\right)'\right)'$ are excluded ($T^{ns}*$, gray dots; see Equation 9). The climatology is also indicated (blue). (b) Modeled freshwater flux between the ice and ocean, due to ice melt or ice formation. (c) Reynolds decomposition of the surface HF, following Equation 6: the total surface HF (black line) is the sum of its climatology (blue), the anomalies due to the surface HF only (green), the anomalies due to the variations of the mixed layer depth only, a.k.a. the shoaling term (red) and the covariance between both anomalies (purple). (d) Location of the tile analyzed here (black dot). Note that this tile is slightly northward of the one analyzed in Figure 2, to better illustrate the potential influence of the mixed layer shoaling.

3.4. Can Ice Melt Enhance a Marine Heatwave?

The asymmetry of the dominating MHWs process between onset and decay highlights differences in the mechanisms at play. The overwhelming dominance of the surface HF during onset in ice-melt conditions (triggering over 75% of those MHWs) raises the question of a potential feedback mechanism that could explain this. The albedo feedback is a typical suspect and the lateral advection of warm waters triggering the onset of ice melt and therefore of an albedo feedback event has been documented in the Chukchi Sea (Woodgate et al., 2010). According to the geographical distribution of MHWs onset by lateral advection (Figure 5), such events can be expected in the Chukchi Sea, but also in Baffin Bay and north of the Barents Sea Opening.

Another potential feedback mechanism is related to ice melt. The stratification induced by meltwater tends to shoal the mixed layer, leading to a smaller volume to heat and therefore facilitating the onset of an MHW. The MHW would in turn generate more ice melt, therefore inducing a positive feedback loop. This mechanism has been hypothesized by other studies (Hu et al., 2020) but not demonstrated because of the lack of available mixed layer observations. The model outputs can provide critical information to corroborate or refute the existence of such an ice melt—MHW positive feedback. To this aim, a Reynolds decomposition of the surface HF is conducted, as described in Section 2.4.

The terms of interest (from Equation 6) to determine the role of ice melt in the onset of an MHW are those related to the anomalous mixed layer depth, called hereafter the shoaling term $\overline{F_{\text{surf}}}\left(\frac{1}{H}\right)'$ (note that this shoaling term can also encompass deepening of the mixed layer, though the Marine Heatwave Tracker this is rarely the case in this context) and the covariance term $\left(F'_{\text{surf}}\left(\frac{1}{H}\right)'\right)'$ (Figure 6c, red and purple lines). The first term accounts for changes of the mixed layer heat input due to the shoaling, if climatological surface HF was applied, while the second term looks at the correlated impact of the mixed layer shoaling projected onto the anomalies of surface HF. The respective contributions of those terms to the mixed layer temperature anomalies can be calculated by dividing by $\rho_0 c_p$ and integrating over the MHW duration, then removed from the mixed layer temperature to obtain an expected temperature without mixed layer shoaling (see Equations 7 and 9). In the case of the modeled summer 2020 Siberian MHW, the ice melt occurring in June and beginning of July (Figure 6b) creates an anomalous shoaling of the mixed layer, but is not enough to compensate the anomalous negative surface flux (Figure 6c, green line) which leads to colder than climatological conditions (Figures 6a and 6c, black line). The fast warming of the mixed layer starts early July with the positive HF anomaly (the mixed layer depth anomaly is close to 0), until the mixed layer temperature exceeds the threshold on the 25 July, marking the beginning of the MHW at this location. It is interesting to note that the surface flux anomaly decreases after that date but is partly compensated by the mixed layer depth anomaly increase, sustaining the MHW. In other words, ice melt—mixed layer depth shoaling feedback helps to lengthen the MHW after it has been initiated. When removing this shoaling-generated warming from the mixed layer temperature, the resulting anomalous temperature still results in an MHW, but does not reach the same peak value and drops below the threshold 11 days earlier than in the actual temperature (Figure 6a, dashed black and dotted gray lines). The impact can even be seen for the rest of the summer, with the second MHW also reaching lower intensity and duration, or even not happening at all if including the covariance of shoaling and surface HF anomalies $\left(F'_{\text{surf}}\left(\frac{1}{H}\right)'\right)'$. Nonetheless, the dominant process driving the MHW onset remains the surface flux anomaly. The term encompassing the mixed layer depth anomaly increases while the melt flux goes back to 0, indicating that there is no ice to melt anymore, but this doesn't discard the previous ice melt as a main reason for the shoaling, since the anomalies are relative to the climatology. While the shoaling could be due to several physical processes, including lower wind mixing, the wind stress doesn't exhibit any significant anomalies during July 2020 (not shown).

The focus on this specific event is instructive on the relative behaviors of the decomposed terms, but it does not provide a robust conclusion on the overall impact of ice melt onto the surface HF. Following a similar approach as with the heat budget process ranking, each of the Reynolds decomposition term can be integrated during the onset of each MHW and then ranked. According to this calculation, the vast majority (88%) of the modeled MHWs whose onset is triggered by the surface heat term are dominated by the surface HF anomaly $F'_{\text{surf}}\overline{\frac{1}{H}}$, while the rest (12%) are driven by the mixed layer anomaly term $\overline{F_{\text{surf}}}\left(\frac{1}{H}\right)'$; the third term, accounting for the covariance of both anomalies, is nearly always negligible when ranking drivers. The ice melt—MHW feedback therefore doesn't seem to be a significant process in the onset of extreme temperature events in the Arctic Ocean. But as demonstrated in the specific case of the Siberian MHW, the shoaling can extend and intensify MHWs. Using the same approach as earlier, $\overline{F_{\text{surf}}}\left(\frac{1}{H}\right)'$ and $\left(F'_{\text{surf}}\left(\frac{1}{H}\right)'\right)'$ can be converted into mixed layer temperature contributions and removed from the actual temperature, to then estimate the change on the MHW properties. Removing the first term only or both can provide bounds on the impact of ice-induced mixed layer shoaling. When conducting this analysis on the 335 MHWs that are primarily driven by surface HF and during whose onset the shoaling term is positive, it can be calculated that 10%–15% of those MHWs have a duration that drops below the 5 days limit in the absence of mixed-layer shoaling, meaning those would not be considered as MHWs anymore (consistent with the previous estimate of 12% of MHWs triggered by the mixed layer depth anomaly). More importantly, the mean duration is reduced by 18%–25%, the mean intensity by 19% (19.1% and 18.6% for each method, respectively) and the cumulative intensity by 29%–31% (Figure S5 in Supporting Information S1). The shoaling term has a limited impact on the peak intensity, reducing it by 1%–5% only. This indicates that these simulated MHWs are primarily triggered by surface HF anomalies but are then prolonged by the shoaling term.

3.5. Salinity-Induced Trends of Winter Arctic Temperature

The presence of sea ice in the Arctic Ocean is due to its β-stratification, induced by salinity rather than temperature as is the case in most of the world ocean. This β-stratification is controlled by high freshwater inputs predominantly from Arctic river discharge (Carmack, 2007). As a consequence, the winter temperature reaches

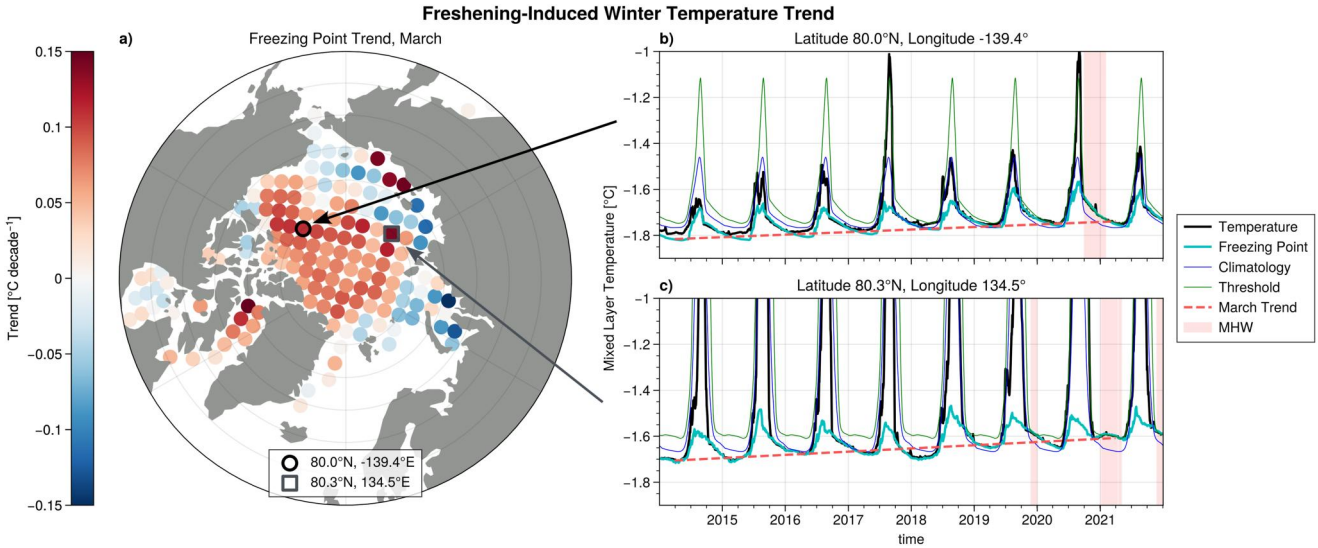

Figure 7. Impact of the Arctic freshening onto the mixed layer winter temperature and on winter marine heatwaves. (a) Map of the trends of the freezing point in the mixed layer in March, due to the Arctic salinity trend, for each of the tiles of the domain of the NAPA model (dots). Two representative examples are illustrated, for (b) the central Beaufort Gyre (black circle) and (c) the Laptev Sea (gray square), showing the mixed layer temperature (black line), the climatology (blue line), the 90th percentile threshold (green line), the freezing point calculated from surface salinity (light blue line) and the periods when this freezing point exceeds the MHW detection threshold (red areas). The increasing trend for the freezing point in March is also shown (red dashed line).

the freezing point, which is a function of salinity. The winter temperature is therefore salinity-constrained, leading to interesting considerations on the role of salinity in the presence of MHWs in the Arctic.

In the framework provided by Hobday et al. (2016), an MHW is defined as temperature excess relative to the 90th percentile. If the winter temperature is consistently near the freezing point, the threshold would be very close to the climatology. Even small departures of the winter temperature from this climatology would therefore match the definition of an MHW. Such a small departure could be induced by vertical mixing with warmer subsurface waters, or by transient eddies. Another cause for such a departure could be a long-term trend in the salinity, since such a trend would change the freezing point. The Arctic Ocean has been steadily freshening over the last two decades at least (e.g., Brown et al., 2020; Proshutinsky et al., 2019), leading to a higher freezing point and thus rising wintertime surface temperatures.

Using the mixed-layer salinity from the model, the freezing point can be calculated over the Arctic. The ice-covered temperature closely follows the calculated freezing point, providing confidence that salinity is controlling the winter temperature over the Arctic Ocean in the NAPA model (Figure 7). The simulated freshening in March (month of maximum ice extent) over 2014–2021 is of the order of 1 psu per decade in the Central Arctic Ocean (North of 80°N) and leads to an increasing trend of the freezing point of up to 0.1°C per decade over most of the central Arctic Ocean, with some spatial variation. The Siberian shelves, including the Chukchi, Laptev and Kara Seas exhibit a decreasing trend, particularly close to the main river estuaries, but the climatology-based treatment of river runoff in the model might limit the robustness of the trend calculation in those areas. Superimposed on the linear trend, interannual variability of salinity also affects the freezing point and complicates the interpretation of winter MHWs (e.g., Figure 7b).

The freshening-induced increasing trend alone, of a magnitude close to 0.1°C per decade, is enough to occasionally raise the winter temperature above the threshold (Figures 7a and 7b, red periods). In other words, those specific MHWs are triggered not by a HF, but by a freshwater flux. The introduction of the criteria on MHW intensity relative to the climatology is enough to discard those events in most cases, but not always (Figure S1 in Supporting Information S1). The relevance of those events is discussed in the next section.

4. Discussion and Conclusion

Processes leading to MHWs in the Arctic Ocean are elucidated using a coupled ice-ocean model and a surface mixed layer heat budget approach for the onset and decay of the extreme temperature events. The seasonality and

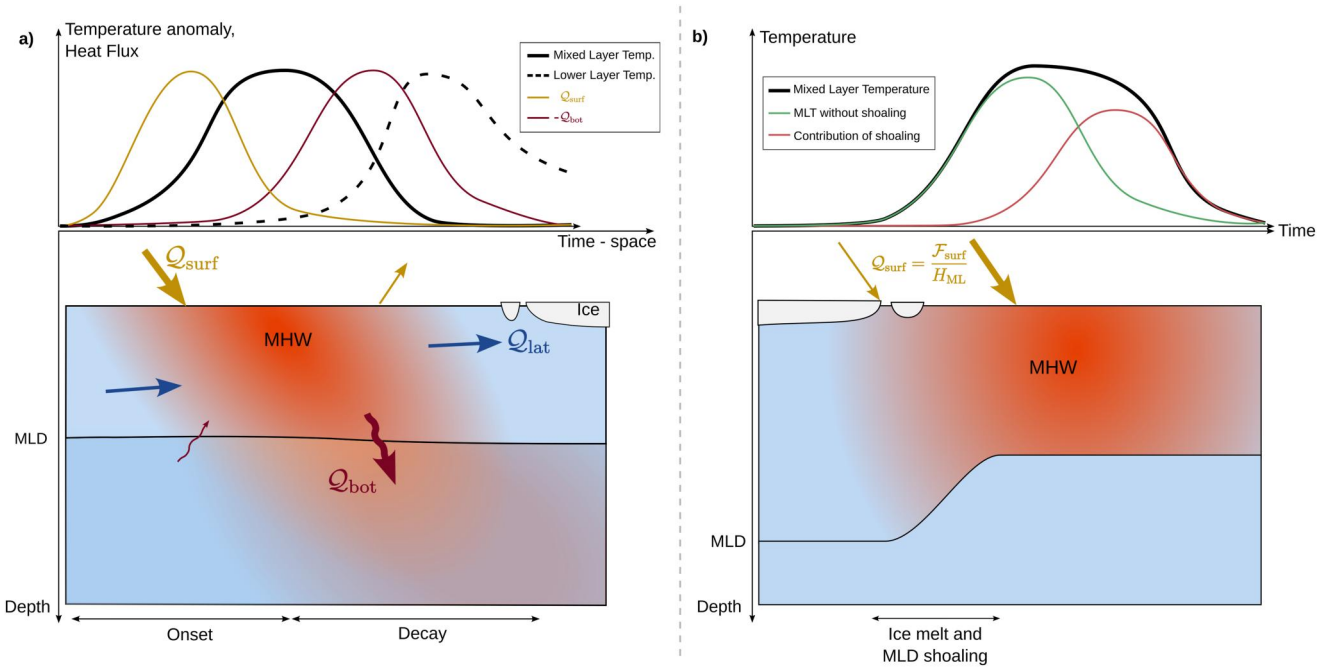

Figure 8. Conceptual summary of the primary methods of formation and decay of marine heatwaves (MHWs) in the Arctic Ocean. (a) Schematic view of the life of an Arctic MHW: surface heat flux (HF) (yellow) initiates positive mixed layer temperature anomalies dissipated by bottom HF (dark red) that can lead to positive subsurface temperature anomalies; lateral heat fluxes (blue) can also play a role in triggering and dissipating MHWs. (b) Shoaling of the mixed layer due to ice melt, leading to an MHW; conceptual description of the contribution of ice-induced shoaling (red line) onto mixed layer temperature (black line) and shape of an MHW without it (green line). MLD stands for Mixed Layer Depth and MLT for Mixed Layer Temperature.

geographic distribution are revealed, including relations with the ice-ocean melt flux. The surface HF, dominated by atmospheric HF, is the main process for the onset of most (two thirds) of the detected MHWs, over the whole Arctic and at all seasons, except during freezing conditions when lateral advection becomes the dominating process, along with bottom HF. MHWs are mainly dissipated by the bottom HF, through vertical mixing and entrainment, with the exception of freezing conditions when heat is lost at the surface to the cold atmosphere or the sea ice. Lateral advection is the main secondary process in both onset and decay.

With the Arctic Amplification leading the Arctic Ocean from a perennially toward a seasonally ice-covered ocean, the role of the surface HF can be expected to gain in importance for the onset of MHWs, with more and more open waters and therefore a strengthening of the albedo feedback. Most of the Arctic MHWs are already driven by surface HF and this can be expected to increase. It is worth noting that due to this albedo feedback, along with the strong stability of the lower Arctic atmosphere, the dominant part of the surface HF is composed of the solar and longwave radiation and not the sensible HF driven by the surface air temperature, in line with the scientific literature (Serreze et al., 2007) and contrary to what has been suggested recently (Huang, Wang, et al., 2021).

The dissipation of MHWs exhibits seasonal and geographic variability, but is mainly a consequence of bottom HF, over most of the Arctic, according to our model. Subsurface waters are dominantly colder than the surface mixed layer waters during MHWs, cooling the mixed layer when mixing with it. The reduced sea ice concentration can increase wind mixing (Rippeth & Fine, 2022) and the retreat of the ice edge over continental shelves can induce downwelling (Carmack & Chapman, 2003). The Beaufort Gyre and the Chukchi Sea are an interesting exception, where the β-stratification of the Arctic allows for the presence of the Near Surface Temperature Maximum, a seasonal warm layer of water sitting below the mixed layer and heated by solar radiation penetrating deeper than the halocline in the oligotrophic waters (Jackson et al., 2010). While our model reproduces well the existence of this Near Surface Temperature Maximum, its geographic extent is more constrained than in other studies (e.g., Steele et al., 2011, not shown). Its presence means that any vertical mixing would occur with warm waters, reducing the potential for cooling the mixed layer, and therefore explains well the reduced bottom dissipation and even the onset of MHWs, specifically in winter, over the Chukchi Sea and the south-western side

of the Beaufort Gyre. For the eastern side of the Beaufort Gyre, though, its absence in our model does not explain the lack of bottom dissipation. Two main reasons can explain this: the first is the very small number of MHWs in this area (Figure 3c), the second is the denser ice pack which reduces the wind-induced vertical mixing.

For most of the Arctic Ocean, and particularly for spring and summer seasons, simulated MHWs are mainly triggered by surface HF and dissipated by bottom HF, therefore providing a pathway for heat from the atmosphere to the subsurface (Figure 8a). Out of the 923 MHWs detected, 302 are predominantly triggered by surface and dissipated by bottom heat fluxes, while 237 are seeing the surface HF dominating for both onset and decay. The rest is divided among the other cases. The surface triggered and bottom dissipated MHWs, which represent 33% of the total, are overall shorter but more intense than the other types of MHWs (not shown). A quantification of the associated energy validates this higher intensity and supports a transfer of heat to the subsurface ocean for this category of MHWs. This heat could be either stored on the long term in the underlying waters (Pacific Summer waters over the Amerasian Basin, Atlantic waters over the Eurasian Basin) or reinjected in the mixed layer in winter when the mixed layer deepens during ice formation. The impact of stored solar heat on sea ice has been documented (e.g., Smith et al., 2018; Timmermans, 2015; Timmermans et al., 2018). The physical impacts of MHWs can be hypothesized to be similar, yet more extreme by definition. MHWs that are triggered and dissipated by surface HF represent 26% of the total and are overall longer but less intense than average (not shown). Those MHWs act as a temporary storage of atmospheric heat in the surface ocean. MHWs that are onset by surface HF, laterally advected to another area to then be dissipated by surface HF would play the same role, though this spatial evolution is more complicated to follow and is outside the scope of this study.

In spring, the ice melt shoals the mixed layer and is therefore hypothesized to concentrate the atmospheric heat, potentially leading to MHWs and more ice melt (Figure 8b). Our results support part of this hypothesis: conceptually, the surface HF anomaly is the determining factor for triggering the timing and peak of an MHW, but the shoaling prolongs it beyond its expected decay. As mentioned earlier, the atmospheric HF is mostly due to solar radiation, which can penetrate deeper than the mixed layer in oligotrophic waters. This process is at the root of the Near Surface Temperature Maximum in the Chukchi Sea and the southern parts of the Amerasian Basin (Jackson et al., 2010; Steele et al., 2011). Therefore, the impact of melt-induced shoaling on the heat input in the surface mixed layer is likely to be limited. Nonetheless, the Reynolds decomposition of the surface HF does support the existence of a noticeable impact, as the shoaling of the mixed layer is responsible for 18%–25% of the MHW duration and increases their mean intensity significantly (Figure S5 in Supporting Information S1). It is also the dominating process for the onset of 12% of the surface-driven MHWs. Here, the impact of shoaling on MHW metrics is only accounted for during the MHW itself (see Section 2.4), but preconditioning could also be significant. Integrating the mixed layer shoaling effect from the beginning of the ice melt rather than the during the MHW would lead to even more important changes in the MHW properties, as would integrating the shoaling effect over the whole summer period if several MHWs are occurring during one summer. This is well illustrated in the case of the summer 2020 Siberian MHW, for which the second MHW would not even occur if the contribution of both shoaling effect terms was removed from the temperature tendency from the start of the first MHW until the end of the second one (Figure 6a, dotted gray line). The estimates provided in this study should therefore be considered as conservative. A limitation of this analysis is that, while we are confident that the shoaling is mostly due to ice melt in the β-stratified Arctic Ocean, we cannot exclude the influence of wind mixing, precipitation or other processes leading to a change in the stratification. The methodology developed in this modeling study could prove helpful in other, thermally stratified parts of the global ocean to disentangle the self-reinforcing effect of surface MHWs strengthening the mixed layer stratification. It is also worth mentioning that in eutrophic waters on the Eurasian side of the Arctic Ocean, the ice melt-induced stratification may generate phytoplankton blooms and reduce the efficiency of the vertical sinking of organic matter, increasing organic matter concentration in the surface and allowing for more solar radiation absorption at the surface. While we do not resolve the biologically driven absorption changes, this process is unlikely to significantly impact the results of this study.

The temperature anomalies can be advected, especially on the shelves and northward of the main Arctic gateways following the general oceanic circulation features (e.g., Rudels & Carmack, 2022). This has been found to trigger ice melt and the onset of an albedo feedback loop north of the Bering Strait (Woodgate et al., 2010). Our analysis supports those findings and provides the location of further hotspots where such processes could regularly occur, including the Barents Sea Opening, the Siberian Shelves and Baffin Bay. Therefore, upstream MHWs should be considered as a potential source of basal melt or of ice formation delay when investigating sea ice seasonality changes.

MHWs in seasonally ice-covered oceans present specific challenges to properly define and detect them. In this study, we use a relatively short time series of 8 years, compared to the recommended 30 years (Hobday et al., 2016). Other studies have used short time series with success (e.g., Oliver et al., 2017). It has also been shown that using 10 years provides MHWs that "are not appreciably different from the MHWs detected with 30 years" (Schlegel et al., 2019). Moreover, the characteristics of Arctic MHWs detected using the short baseline (Figure 3) matches the spatial patterns provided by other studies using a longer baseline (e.g., Huang, Wang, et al., 2021), despite differences in the products used (modeled mixed-layer temperature compared to satellite-derived SST). Using SST from OISSTv2.1, it can be seen that using a 30-year baseline lowers the threshold compared to using an 8-year baseline over recent years. This effect is due to the long-term warming trend, particularly important in the Arctic region. The detected MHWs are longer and more intense when using a longer baseline (Figure S6 in Supporting Information S1). The drivers of the longer MHWs could be decomposed into a component related to the long-term warming and a component related to oscillations around the warming. With a shorter baseline, only the latter component is captured. It can be expected that the surface HF forcing for MHW onset would likely be more important with a longer baseline, as it would include more of the long-term albedo feedback and atmospheric warming. It is less obvious to estimate how the decay drivers would change when using a longer baseline. The observed warming of the subsurface Pacific and Atlantic waters (Timmermans & Marshall, 2020) could be an indication of increased downward vertical heat transport, especially on the shelves (Timmermans et al., 2018), but could also reduce the capacity of the surface mixed layer to export heat below on the long term, as the temperature differential diminishes. On the other hand, a more mobile ice pack can increase wind-induced vertical mixing, but the direction of the associated HF would depend on the vertical temperature gradient. A change of the baseline for the Siberian MHW presented in Section 3.1 hints toward a stronger surface HF for the onset and a stronger bottom HF for the decay (not shown), but further investigation is necessary to properly fill this knowledge gap. The lateral HF would likely be impacted as well. During onset and using a longer baseline, this term might increase at the Arctic gateways, as it would incorporate more of the long-term increased heat transport from Atlantic and Pacific into the Arctic. Its role during MHWs decay could also increase, as the more mobile ice pack in recent decades would allow more lateral exchanges in the marginal ice zone with freezing waters. It should be pointed out that as the threshold is defined using the 90th percentile, and because the warmer years are recent years in the context of a fast-warming Arctic, a long and a short baseline will capture a relatively similar threshold (the distribution tail would be similar), despite the climatologies being potentially different.

Another difficulty to detect MHWs in the Arctic is related to the highly stable temperature in winter conditions, which leads to a threshold close to the climatology. A shortened ice season means that the earlier open water conditions are quickly detected as MHWs. While some studies tend to restrain their scope to summer MHWs or introduce a high, summer-defined threshold, we kept all MHWs that exceed the mixed layer temperature climatology by more than 0.1°C. Despite this threshold added to the classic definition (Hobday et al., 2016), some of the detected MHWs still occur in winter in ice-covered conditions, due to the increasing trend of the freezing point related to the freshening of the Arctic. Considering that the freshening of the Arctic has been observed for several decades (Rudels & Carmack, 2022), using a longer baseline would increase the number of those winter MHWs and lengthen them. Detrending the time series for each day of the year would likely be a solution to get rid of the freshening-induced MHWs, if this was desired. The literature on decadal trends of the winter mixed layer temperature in the Arctic is scarce due to the lack of in-situ and satellite observations in ice-covered regions. The Arctic is therefore often blanked out (e.g., Meredith et al., 2019), but the few available estimates are in line with a trend of 0.1°C per decade (J.-L. Chen et al., 2019; Fox-Kemper et al., 2021). The higher winter temperature does not only trigger MHWs in the winter, but also raises the starting point of the seasonal cycle, meaning that for identical seasonal heat forcing, the summer maximum temperature will also be higher, potentially increasing the number of summer MHWs. The general warming trend is also an issue in other seasons, but those have been better studied, especially in other parts of the global ocean (Oliver, 2019).

The relevance of cold season MHWs is difficult to quantify. They may have physical consequences on ice growth and melt and on the rest of the seasonal cycle, which shouldn't be overlooked. Their biological and biogeochemical impacts are beyond the scope of this study, but it should be noted that the temperature and salinity of sea ice control the sympagic (i.e., inside the ice) carbonate cycling (e.g., Delille et al., 2014; Moreau et al., 2015). Moreover, ecosystems adapted to the stable Arctic environment cannot shift their latitudinal range, contrarily to what is seen at other latitudes. On the other hand, a warming baseline can expand the habitat of some species, such as kelp (Goldsmit et al., 2021). The impact of MHWs on

ecosystems is a thriving topic for the rest of the global ocean (Hobday et al., 2018; Oliver et al., 2019; Smale et al., 2019) and specific events have been regularly documented, whether during the North Pacific "Blob" (Walsh et al., 2018), the 2003 Mediterranean MHW (Garrabou et al., 2009) or the Tasmanian MHW of 2015–2016 (Oliver et al., 2017). In the Arctic as well, some studies have identified immediate responses of fish to extreme events (Husson et al., 2022) and the complex but important ecological consequences of sea ice loss are an active field of research (e.g., Arrigo & van Dijken, 2011; Lannuzel et al., 2020). Studies disentangling the impact of the extreme events from the amplified Arctic trend on the local ecosystems are scarcer but highly needed, including those dedicated to benthic ecosystems that could be vulnerable to the subsurface fate of heat uncovered in this study.

Appendix A: Reynolds Decomposition

Because $\rho_0 c_p$ is constant, the decomposition is restrained to the $\frac{F_{surf}}{H}$ term:

$$\begin{aligned}\frac{F_{surf}}{H} &= \left(\overline{F_{surf}} + F'_{surf}\right)\left(\overline{\frac{1}{H}} + \left(\frac{1}{H}\right)'\right) \\ &= \overline{F_{surf}}\,\overline{\frac{1}{H}} + F'_{surf}\,\overline{\frac{1}{H}} + \overline{F_{surf}}\left(\frac{1}{H}\right)' + F'_{surf}\left(\frac{1}{H}\right)'\end{aligned} \tag{A1}$$

The first term on the rhs is the climatology of the surface heat flux (HF) in the mixed layer, the second term, called the HF anomaly term, accounts for the anomaly of heat due to changes in the HF only, the third term, called the shoaling term, accounts for the heat anomaly due to changes in the mixed layer depth only and the last term represents influence of co-occurring anomalous changes in both the surface HF and the mixed layer depth. The time-mean of this last term is not null, though it is very small and could be neglected (not shown):

$$\begin{aligned}F'_{surf}\left(\frac{1}{H}\right)' &= \overline{F'_{surf}\left(\frac{1}{H}\right)'} + \left(F'_{surf}\left(\frac{1}{H}\right)'\right)' \\ &\approx \left(F'_{surf}\left(\frac{1}{H}\right)'\right)'\end{aligned} \tag{A2}$$

The time-mean part of the covariant term $\overline{F'_{surf}\left(\frac{1}{H}\right)'}$ needs to be added to the climatological term of Equation 6 to fully retrieve the climatological surface HF of Equation 5:

$$\overline{Q_{surf}} = \frac{1}{\rho_0 c_p}\overline{\frac{F_{surf}}{H}} = \frac{1}{\rho_0 c_p}\overline{F_{surf}}\,\overline{\frac{1}{H}} + \frac{1}{\rho_0 c_p}\overline{F'_{surf}\left(\frac{1}{H}\right)'} \tag{A3}$$

The other terms of Equation 6 including the anomalies of the covariance term $\left(F'_{surf}\left(\frac{1}{H}\right)'\right)'$ are contributing to the anomalous surface HF

$$Q'_{surf} = \frac{1}{\rho_0 c_p}F'_{surf}\,\overline{\frac{1}{H}} + \frac{1}{\rho_0 c_p}\overline{F_{surf}}\left(\frac{1}{H}\right)' + \frac{1}{\rho_0 c_p}\left(F'_{surf}\left(\frac{1}{H}\right)'\right)' \tag{A4}$$

Similarly to the full heat budget approach, one can integrate each of those terms during the onset and decay of an marine heatwave to get a contribution to the temperature anomalies in °C and therefore determine the dominating mechanism, between the surface HF or the variation of the mixed layer depth.

Data Availability Statement

The ERA5 reanalysis product (Hersbach et al., 2020) was made available through Copernicus Climate Change Service. Processed data and code used for this manuscript are publicly available at https://zenodo.org/doi/10.5281/zenodo.10246840 (Richaud et al., 2023).

Acknowledgments
This work is supported by the National Sciences and Engineering Research Council of Canada Discovery Grant RGPIN-2018-05255, the Ocean Frontier Institute through an award from the Canada First Research Excellence Fund, and ArcticNet, a Network of Centres of Excellence Canada. The authors express their gratitude to three anonymous reviewers and the editor Léon Chafik for their invaluable comments that greatly improved this paper.

References

Arrigo, K. R., & van Dijken, G. L. (2011). Secular trends in Arctic Ocean net primary production. *Journal of Geophysical Research*, *116*(C9), C09011. https://doi.org/10.1029/2011JC007151

Batrak, Y., & Müller, M. (2019). On the warm bias in atmospheric reanalyses induced by the missing snow over Arctic sea-ice. *Nature Communications*, *10*(1), 4170. https://doi.org/10.1038/s41467-019-11975-3

Bekryaev, R. V., Polyakov, I. V., & Alexeev, V. A. (2010). Role of polar amplification in long-term surface air temperature variations and modern Arctic warming. *Journal of Climate*, *23*(14), 3888–3906. https://doi.org/10.1175/2010JCLI3297.1

Beszczynska-Möller, A., Fahrbach, E., Schauer, U., & Hansen, E. (2012). Variability in Atlantic water temperature and transport at the entrance to the Arctic Ocean, 1997–2010. *ICES Journal of Marine Science*, *69*(5), 852–863. https://doi.org/10.1093/icesjms/fss056

Brown, K. A., Holding, J. M., & Carmack, E. C. (2020). Understanding regional and seasonal variability is key to gaining a pan-Arctic perspective on Arctic Ocean freshening. *Frontiers in Marine Science*, *7*. https://doi.org/10.3389/fmars.2020.00606

Carmack, E., & Chapman, D. C. (2003). Wind-driven shelf/basin exchange on an Arctic shelf: The joint roles of ice cover extent and shelf-break bathymetry: WIND-DRIVEN SHELF/BASIN EXCHANGE. *Geophysical Research Letters*, *30*, 14. https://doi.org/10.1029/2003GL017526

Carmack, E., Polyakov, I., Padman, L., Fer, I., Hunke, E., Hutchings, J., et al. (2015). Toward quantifying the increasing role of oceanic heat in Sea Ice loss in the new Arctic. *Bulletin of the American Meteorological Society*, *96*(12), 2079–2105. https://doi.org/10.1175/BAMS-D-13-00177.1

Carmack, E. C. (2007). The alpha/beta ocean distinction: A perspective on freshwater fluxes, convection, nutrients and productivity in high-latitude seas. *Deep Sea Research Part II: Topical Studies in Oceanography*, *54*(23), 2578–2598. https://doi.org/10.1016/j.dsr2.2007.08.018

Carvalho, K. S., Smith, T. E., & Wang, S. (2021). Bering Sea marine heatwaves: Patterns, trends and connections with the Arctic. *Journal of Hydrology*, *600*, 126462. https://doi.org/10.1016/j.jhydrol.2021.126462

Chen, J.-L., Kang, S.-C., Meng, X.-H., & You, Q.-L. (2019). Assessments of the Arctic amplification and the changes in the Arctic sea surface. *Advances in Climate Change Research*, *10*(4), 193–202. https://doi.org/10.1016/j.accre.2020.03.002

Chen, K., Gawarkiewicz, G., Kwon, Y.-O., & Zhang, W. G. (2015). The role of atmospheric forcing versus ocean advection during the extreme warming of the Northeast U.S. continental shelf in 2012. *Journal of Geophysical Research: Oceans*, *120*(6), 4324–4339. https://doi.org/10.1002/2014JC010547

Ciavarella, A., Cotterill, D., Stott, P., Kew, S., Philip, S., van Oldenborgh, G. J., et al. (2021). Prolonged Siberian heat of 2020 almost impossible without human influence. *Climatic Change*, *166*(1), 9. https://doi.org/10.1007/s10584-021-03052-w

Coles, S. (2001). *An introduction to statistical modeling of extreme values*. Springer. https://doi.org/10.1007/978-1-4471-3675-0

Dai, A., & Trenberth, K. E. (2002). Estimates of freshwater discharge from continents: Latitudinal and seasonal variations. *Journal of Hydrometeorology*, *3*(6), 660–687. https://doi.org/10.1175/1525-7541(2002)003<0660:EOFDFC>2.0.CO;2

Delille, B., Vancoppenolle, M., Geilfus, N.-X., Tilbrook, B., Lannuzel, D., Schoemann, V., et al. (2014). Southern Ocean CO_2 sink: The contribution of the sea ice. *Journal of Geophysical Research: Oceans*, *119*(9), 6340–6355. https://doi.org/10.1002/2014JC009941

Docquier, D., & Koenigk, T. (2021). A review of interactions between ocean heat transport and Arctic sea ice. *Environmental Research Letters*, *16*(12), 123002. https://doi.org/10.1088/1748-9326/ac30be

Dussin, R., Barnier, B., Brodeau, L., & Molines, J.-M. (2016). The making of the Drakkar forcing set DFS5. *Zenodo*. https://doi.org/10.5281/zenodo.1209243

Ferry, N., Parent, L., Garric, G., Bricaud, C., Testut, C., Le Galloudec, O., et al. (2012). GLORYS2V1 global ocean reanalysis of the altimetric era (1992–2009) at meso scale. *Mercator Ocean–Quaterly Newsletter*, *44*, 29–39.

Fox-Kemper, B., Hewitt, H., Xiao, C., Adhalgeirsdóttir, G., Drijfhout, S., Edwards, T., et al. (2021). Ocean, cryosphere and sea level change. In V. Masson-Delmotte, P. Zhai, A. Pirani, S. L. Connors, C. Péan, S. Berger, et al. (Eds.), *Climate change 2021: The physical science basis. Contribution of working group I to the sixth assessment report of the intergovernmental panel on climate change* (pp. 1211–1362). Cambridge University Press. https://doi.org/10.1017/9781009157896.011

Frölicher, T. L., Fischer, E. M., & Gruber, N. (2018). Marine heatwaves under global warming. *Nature*, *560*(7718), 360–364. https://doi.org/10.1038/s41586-018-0383-9

Garrabou, J., Coma, R., Bensoussan, N., Bally, M., Chevaldonné, P., Cigliano, M., et al. (2009). Mass mortality in Northwestern Mediterranean rocky benthic communities: Effects of the 2003 heat wave. *Global Change Biology*, *15*(5), 1090–1103. https://doi.org/10.1111/j.1365-2486.2008.01823.x

Goldsmit, J., Schlegel, R. W., Filbee-Dexter, K., MacGregor, K. A., Johnson, L. E., Mundy, C. J., et al. (2021). Kelp in the eastern Canadian Arctic: Current and future predictions of habitat suitability and cover. *Frontiers in Marine Science*, *8*, 742209. https://doi.org/10.3389/fmars.2021.742209

Golubeva, E., Kraineva, M., Platov, G., Iakshina, D., & Tarkhanova, M. (2021). Marine heatwaves in Siberian Arctic seas and adjacent region. *Remote Sensing*, *13*(21), 4436. https://doi.org/10.3390/rs13214436

Goosse, H., Kay, J. E., Armour, K. C., Bodas-Salcedo, A., Chepfer, H., Docquier, D., et al. (2018). Quantifying climate feedbacks in polar regions. *Nature Communications*, *9*(1), 1919. https://doi.org/10.1038/s41467-018-04173-0

Hall, A. (2004). The role of surface albedo feedback in climate. *Journal of Climate*, *17*(7), 1550–1568. https://doi.org/10.1175/1520-0442(2004)017⟨1550:TROSAF⟩2.0.CO;2

Hersbach, H., Bell, B., Berrisford, P., Hirahara, S., Horányi, A., Muñoz-Sabater, J., et al. (2020). The ERA5 global reanalysis. *Quarterly Journal of the Royal Meteorological Society*, *146*(730), 1999–2049. https://doi.org/10.1002/qj.3803

Hobday, A. J., Alexander, L. V., Perkins, S. E., Smale, D. A., Straub, S. C., Oliver, E. C., et al. (2016). A hierarchical approach to defining marine heatwaves. *Progress in Oceanography*, *141*, 227–238. https://doi.org/10.1016/j.pocean.2015.12.014

Hobday, A. J., Oliver, E., Sen Gupta, A., Benthuysen, J., Burrows, M., Donat, M., et al. (2018). Categorizing and naming marine heatwaves. *Oceanography*, *31*(2), 62. https://doi.org/10.5670/oceanog.2018.205

Holbrook, N. J., Scannell, H. A., Sen Gupta, A., Benthuysen, J. A., Feng, M., Oliver, E. C. J., et al. (2019). A global assessment of marine heatwaves and their drivers. *Nature Communications*, *10*(1), 2624. https://doi.org/10.1038/s41467-019-10206-z

Hu, S., Zhang, L., & Qian, S. (2020). Marine heatwaves in the Arctic region: Variation in different ice covers. *Geophysical Research Letters*, *47*(16), e2020GL089329. https://doi.org/10.1029/2020GL089329

Huang, B., Liu, C., Banzon, V., Freeman, E., Graham, G., Hankins, B., et al. (2021). Improvements of the daily optimum interpolation sea surface temperature (DOISST) version 2.1. *Journal of Climate*, *34*(8), 2923–2939. https://doi.org/10.1175/JCLI-D-20-0166.1

Huang, B., Wang, Z., Yin, X., Arguez, A., Graham, G., Liu, C., et al. (2021). Prolonged marine heatwaves in the Arctic: 1982–2020. *Geophysical Research Letters*, *48*(24), e2021GL095590. https://doi.org/10.1029/2021GL095590

Husson, B., Lind, S., Fossheim, M., Kato-Solvang, H., Skern-Mauritzen, M., Pécuchet, L., et al. (2022). Successive extreme climatic events lead to immediate, large-scale, and diverse responses from fish in the Arctic. *Global Change Biology*, *28*(11), 3728–3744. https://doi.org/10.1111/gcb.16153

IPCC. (2021). *Climate change 2021: The physical science basis. Contribution of working group I to the sixth assessment report of the intergovernmental panel on climate change*. Cambridge University Press. https://doi.org/10.1017/9781009157896

Ivanov, V., Alexeev, V., Koldunov, N. V., Repina, I., Sandø, A. B., Smedsrud, L. H., & Smirnov, A. (2016). Arctic Ocean heat impact on regional ice decay: A suggested positive feedback. *Journal of Physical Oceanography*, *46*(5), 1437–1456. https://doi.org/10.1175/JPO-D-15-0144.1

Jackson, J. M., Carmack, E. C., McLaughlin, F. A., Allen, S. E., & Ingram, R. G. (2010). Identification, characterization, and change of the near-surface temperature maximum in the Canada Basin, 1993–2008. *Journal of Geophysical Research*, *115*(C5), C05021. https://doi.org/10.1029/2009JC005265

Lannuzel, D., Tedesco, L., van Leeuwe, M., Campbell, K., Flores, H., Delille, B., et al. (2020). The future of Arctic sea-ice biogeochemistry and ice-associated ecosystems. *Nature Climate Change*, *10*(11), 983–992. https://doi.org/10.1038/s41558-020-00940-4

Lique, C., Johnson, H. L., & Plancherel, Y. (2018). Emergence of deep convection in the Arctic Ocean under a warming climate. *Climate Dynamics*, *50*(9), 3833–3847. https://doi.org/10.1007/s00382-017-3849-9

Madec, G., Bourdallé-Badie, R., Bouttier, P.-A., Bricaud, C., Bruciaferri, D., Calvert, D., et al. (2017). NEMO ocean engine. In *Notes du Pôle de modélisation de l'Institut Pierre-Simon Laplace (IPSL)* (Vol. 27). https://doi.org/10.5281/zenodo.3248739

Meier, W., & Stroeve, J. (2022). An updated assessment of the changing Arctic Sea Ice cover. *Oceanography*, *35*, 10–19. https://doi.org/10.5670/oceanog.2022.114

Meredith, M., Sommerkorn, M., Cassotta, S., Derksen, C., Ekaykin, A., Hollowed, A., et al. (2019). Polar regions. In H.-O. Pörtner, D. C. Roberts, V. Masson-Delmotte, P. Zhai, M. Tignor, E. Poloczanska, et al. (Eds.), *IPCC special report on the ocean and cryosphere in a changing climate* (pp. 203–320). Cambridge University Press.

Mohamed, B., Nilsen, F., & Skogseth, R. (2022). Marine heatwaves characteristics in the Barents Sea based on high resolution satellite data (1982–2020). *Frontiers in Marine Science*, *9*, 821646. https://doi.org/10.3389/fmars.2022.821646

Moisan, J. R., & Niiler, P. P. (1998). The seasonal heat budget of the North Pacific: Net heat flux and heat storage rates (1950–1990). *Journal of Physical Oceanography*, *28*(3), 401–421. https://doi.org/10.1175/1520-0485(1998)028<0401:TSHBOT>2.0.CO;2

Moreau, S., Vancoppenolle, M., Delille, B., Tison, J.-L., Zhou, J., Kotovitch, M., et al. (2015). Drivers of inorganic carbon dynamics in first-year sea ice: A model study. *Journal of Geophysical Research: Oceans*, *120*(1), 471–495. https://doi.org/10.1002/2014JC010388

Muilwijk, M., Nummelin, A., Heuzé, C., Polyakov, I. V., Zanowski, H., & Smedsrud, L. H. (2023). Divergence in climate model projections of future Arctic Atlantification. *Journal of Climate*, *36*(6), 1727–1748. https://doi.org/10.1175/JCLI-D-22-0349.1

Olita, A., Sorgente, R., Natale, S., Gaberšek, S., Ribotti, A., Bonanno, A., & Patti, B. (2007). Effects of the 2003 European heatwave on the central mediterranean sea: Surface fluxes and the dynamical response. *Ocean Science*, *3*(2), 273–289. https://doi.org/10.5194/os-3-273-2007

Oliver, E. C. J. (2019). Mean warming not variability drives marine heatwave trends. *Climate Dynamics*, *53*(3), 1653–1659. https://doi.org/10.1007/s00382-019-04707-2

Oliver, E. C. J., Benthuysen, J. A., Bindoff, N. L., Hobday, A. J., Holbrook, N. J., Mundy, C. N., & Perkins-Kirkpatrick, S. E. (2017). The unprecedented 2015/16 Tasman Sea marine heatwave. *Nature Communications*, *8*(1), 16101. https://doi.org/10.1038/ncomms16101

Oliver, E. C. J., Benthuysen, J. A., Darmaraki, S., Donat, M. G., Hobday, A. J., Holbrook, N. J., et al. (2021). Marine heatwaves. *Annual Review of Marine Science*, *13*, 1–30. https://doi.org/10.1146/annurev-marine-032720-095144

Oliver, E. C. J., Burrows, M. T., Donat, M. G., Sen Gupta, A., Alexander, L. V., Perkins-Kirkpatrick, S. E., et al. (2019). Projected marine heatwaves in the 21st century and the potential for ecological impact. *Frontiers in Marine Science*, *6*, 734. https://doi.org/10.3389/fmars.2019.00734

Oliver, E. C. J., Perkins-Kirkpatrick, S. E., Holbrook, N. J., & Bindoff, N. L. (2018). Anthropogenic and natural influences on record 2016 marine heat waves. *Bulletin of the American Meteorological Society*, *99*(1), S44–S48. https://doi.org/10.1175/BAMS-D-17-0093.1

Overland, J. E., & Wang, M. (2021). The 2020 Siberian heat wave. *International Journal of Climatology*, *41*(S1), E2341–E2346. https://doi.org/10.1002/joc.6850

Peralta-Ferriz, C., & Woodgate, R. A. (2015). Seasonal and interannual variability of pan-Arctic surface mixed layer properties from 1979 to 2012 from hydrographic data, and the dominance of stratification for multiyear mixed layer depth shoaling. *Progress in Oceanography*, *134*, 19–53. https://doi.org/10.1016/j.pocean.2014.12.005

Polyakov, I. V., Alkire, M. B., Bluhm, B. A., Brown, K. A., Carmack, E. C., Chierici, M., et al. (2020). Borealization of the Arctic Ocean in response to anomalous advection from sub-Arctic seas. *Frontiers in Marine Science*, *7*, 491. https://doi.org/10.3389/fmars.2020.00491

Polyakov, I. V., Pnyushkov, A. V., Alkire, M. B., Ashik, I. M., Baumann, T. M., Carmack, E. C., et al. (2017). Greater role for Atlantic inflows on sea-ice loss in the Eurasian Basin of the Arctic Ocean. *Science*, *356*(6335), 285–291. https://doi.org/10.1126/science.aai8204

Polyakov, I. V., Rippeth, T. P., Fer, I., Alkire, M. B., Baumann, T. M., Carmack, E. C., et al. (2020). Weakening of cold halocline layer exposes Sea Ice to oceanic heat in the eastern Arctic Ocean. *Journal of Climate*, *33*(18), 8107–8123. https://doi.org/10.1175/JCLI-D-19-0976.1

Proshutinsky, A., Krishfield, R., Toole, J. M., Timmermans, M.-L., Williams, W., Zimmermann, S., et al. (2019). Analysis of the Beaufort Gyre freshwater content in 2003–2018. *Journal of Geophysical Research: Oceans*, *124*(12), 9658–9689. https://doi.org/10.1029/2019JC015281

Rantanen, M., Karpechko, A. Y., Lipponen, A., Nordling, K., Hyvärinen, O., Ruosteenoja, K., et al. (2022). The Arctic has warmed nearly four times faster than the globe since 1979. *Communications Earth & Environment*, *3*(1), 1–10. https://doi.org/10.1038/s43247-022-00498-3

Reynolds, R. W., Rayner, N. A., Smith, T. M., Stokes, D. C., & Wang, W. (2002). An improved in situ and satellite SST analysis for climate. *Journal of Climate*, *15*(13), 1609–1625. https://doi.org/10.1175/1520-0442(2002)015⟨1609:AIISAS⟩2.0.CO;2

Reynolds, R. W., Smith, T. M., Liu, C., Chelton, D. B., Casey, K. S., & Schlax, M. G. (2007). Daily high-resolution-blended analyses for sea surface temperature. *Journal of Climate*, *20*(22), 5473–5496. https://doi.org/10.1175/2007JCLI1824.1

Richaud, B., Hu, X., Darmaraki, S., Fennel, K., Lu, Y., & Oliver, E. C. J. (2023). Data and code for drivers of marine heatwaves in the Arctic Ocean [Dataset]. Zenodo. https://doi.org/10.5281/zenodo.10246841

Rippeth, T., & Fine, E. (2022). Turbulent mixing in a changing Arctic Ocean. *Oceanography*. https://doi.org/10.5670/oceanog.2022.103

Rousset, C., Vancoppenolle, M., Madec, G., Fichefet, T., Flavoni, S., Barthélemy, A., et al. (2015). The Louvain-La-Neuve sea ice model LIM3.6: Global and regional capabilities. *Geoscientific Model Development*, *8*(10), 2991–3005. https://doi.org/10.5194/gmd-8-2991-2015

Rudels, B. (2015). Arctic Ocean circulation, processes and water masses: A description of observations and ideas with focus on the period prior to the international polar year 2007–2009. *Progress in Oceanography*, *132*, 22–67. https://doi.org/10.1016/j.pocean.2013.11.006

Rudels, B., & Carmack, E. (2022). Arctic Ocean water mass structure and circulation. *Oceanography*. https://doi.org/10.5670/oceanog.2022.116

Schlegel, R. W. (2020). Marine heatwave tracker. *Zenodo*. https://doi.org/10.5281/ZENODO.3787872

Schlegel, R. W., Oliver, E. C. J., & Chen, K. (2021). Drivers of marine heatwaves in the northwest Atlantic: The role of air–sea interaction during onset and decline. *Frontiers in Marine Science*, *8*, 627970. https://doi.org/10.3389/fmars.2021.627970

Schlegel, R. W., Oliver, E. C. J., Hobday, A. J., & Smit, A. J. (2019). Detecting marine heatwaves with sub-optimal data. *Frontiers in Marine Science*, *6*, 737. https://doi.org/10.3389/fmars.2019.00737

Schweiger, A. J., Lindsay, R. W., Vavrus, S., & Francis, J. A. (2008). Relationships between Arctic Sea Ice and clouds during Autumn. *Journal of Climate*, *21*(18), 4799–4810. https://doi.org/10.1175/2008JCLI2156.1

Serreze, M. C., Barrett, A. P., Slater, A. G., Steele, M., Zhang, J., & Trenberth, K. E. (2007). The large-scale energy budget of the Arctic. *Journal of Geophysical Research*, *112*(D11), 14. https://doi.org/10.1029/2006JD008230

Serreze, M. C., Barrett, A. P., Stroeve, J. C., Kindig, D. N., & Holland, M. M. (2009). *The emergence of surface-based Arctic amplification*. The Cryosphere.

Smale, D. A., Wernberg, T., Oliver, E. C. J., Mads, T., Harvey, B. P., Straub, S. C., et al. (2019). Marine heatwaves threaten global biodiversity and the provision of ecosystem services. *Nature Climate Change*, *9*(4), 306–312. https://doi.org/10.1038/s41558-019-0412-1

Smith, M., Stammerjohn, S., Persson, O., Rainville, L., Liu, G., Perrie, W., et al. (2018). Episodic reversal of autumn ice advance caused by release of ocean heat in the Beaufort sea. *Journal of Geophysical Research: Oceans*, *123*(5), 3164–3185. https://doi.org/10.1002/2018JC013764

Steele, M., Ermold, W., & Zhang, J. (2011). Modeling the formation and fate of the near-surface temperature maximum in the Canadian Basin of the Arctic Ocean. *Journal of Geophysical Research*, *116*(C11). https://doi.org/10.1029/2010JC006803

Timmermans, M.-L. (2015). The impact of stored solar heat on Arctic sea ice growth. *Geophysical Research Letters*, *42*(15), 6399–6406. https://doi.org/10.1002/2015GL064541

Timmermans, M.-L., & Marshall, J. (2020). Understanding Arctic Ocean circulation: A review of ocean dynamics in a changing climate. *Journal of Geophysical Research: Oceans*, *125*(4), e2018JC014378. https://doi.org/10.1029/2018JC014378

Timmermans, M.-L., Toole, J., & Krishfield, R. (2018). Warming of the interior Arctic Ocean linked to sea ice losses at the basin margins. *Science Advances*, *4*(8), eaat6773. https://doi.org/10.1126/sciadv.aat6773

Walsh, J. E., Thoman, R. L., Bhatt, U. S., Bieniek, P. A., Brettschneider, B., Brubaker, M., et al. (2018). The high latitude marine heat wave of 2016 and its impacts on Alaska. *Bulletin of the American Meteorological Society*, *99*(1), S39–S43. https://doi.org/10.1175/BAMS-D-17-0105.1

Woodgate, R. A. (2018). Increases in the Pacific inflow to the Arctic from 1990 to 2015, and insights into seasonal trends and driving mechanisms from year-round Bering Strait mooring data. *Progress in Oceanography*, *160*, 124–154. https://doi.org/10.1016/j.pocean.2017.12.007

Woodgate, R. A., Weingartner, T., & Lindsay, R. (2010). The 2007 Bering Strait oceanic heat flux and anomalous Arctic sea-ice retreat. *Geophysical Research Letters*, *37*(1), L01602. https://doi.org/10.1029/2009GL041621

Zhang, Y., Wei, H., Lu, Y., Luo, X., Hu, X., & Zhao, W. (2020). Dependence of Beaufort sea low ice condition in the summer of 1998 on ice export in the prior winter. *Journal of Climate*, *33*(21), 9247–9259. https://doi.org/10.1175/JCLI-D-19-0943.1